cylglycine. In this case the bis Co(II) complex of the deprotonated dipeptide is not completely formed unless oxygen is present.

Acknowledgment. This research was supported by the Gas Research Institute, Basic Research Department, under Contract 5014-361-0282.

Registry No. **2a**, 80525-55-9; **2b**, 80525-56-0; **3a**, 88057-06-1; **3b**, 88057-08-3; **4a**, 88057-10-7; **4a**·5HCl, 88057-07-2; **4b**·5HCl, 88057-09-4; bzdien, 23539-10-8; bzdpt, 1555-71-1; 4-benzyl-1,7-diphthaloyldiethylenetriamine, 23538-88-7.

Contribution from the Research School of Chemistry, The Australian National University, Canberra, ACT 2600, Australia, and the Departments of Chemistry and Physics, Monash University, Clayton, Victoria 3168, Australia

Unusual Structural, Chemical, and Magnetic Properties of Mononuclear Iron(III) Complexes of the Potentially Binucleating Ligand *meso*-α,α,α,α-Tetrakis(*o*-nicotinamidophenyl)porphyrin

MAXWELL J. GUNTER,*[1a] GEORGE M. McLAUGHLIN,[1a] KEVIN J. BERRY,[1b] KEITH S. MURRAY,*[1b] MARK IRVING,[1c] and PAUL E. CLARK[1c]

Received October 26, 1982

The preparation and characterization of a series of Fe(III) complexes of the potentially binucleating ligand *meso*-α,α,α,α-tetrakis(*o*-nicotinamidophenyl)porphyrin, FeX(P-N_4), is described (X = Cl, Br, OH, N_3). A crystal structure of FeCl(P-N_4)·$CHCl_3$·H_2O has been determined. Crystal data: space group $P2_1/c$, a = 14.739 (6) Å, b = 21.924 (7) Å, c = 19.524 (6) Å, β = 101.03 (3)°, Z = 4, V = 6192.4 Å^3, 5042 unique reflections, R = 0.104. The structure consists of polymeric chains, with the Fe atom of one molecule coordinated to a pyridine N of the nicotinamide unit of a second molecule. The chloride ion occupies the sixth coordination site, inside the "pocket" of the four nicotinamide groups. The Fe is displaced 0.109 (1) Å from the mean plane of the porphyrin toward the Cl^-. Long Fe–Cl (2.31 (2) Å) and Fe–N_{py} (2.085 (6) Å) distances and an average Fe–N_{porph} distance of 2.042 (8) Å indicate an essentially high-spin Fe, which is accommodated by an S_4 ruffling of the porphyrin. Magnetic susceptibility, ESR, and Mössbauer data on solid samples were interpreted as follows: FeCl(P-N_4)·$CHCl_3$, a mixture of high-spin monomer and high-spin Heisenberg chain, D = 10 ± 0.5 cm^{-1}, E = 2.25 ± 0.25 cm^{-1}, J = −5 ● 0.2 cm^{-1}, fraction of monomer = 0.70 ± 0.02, contributions from spin crossover are also possible; FeBr(P-N_4)·$CHCl_3$ sample 1, containing hexane of solvation, similar to Cl^-, D = 10 cm^{-1}, E = 0.8 cm^{-1}, J = −8 cm^{-1}, α = 0.57; FeBr(P-N_4)·$CHCl_3$, containing no hexane, spin-crossover behavior, g(low-spin state) = 2.21, λ(spin–orbit coupling constant of $^2T_2$ state) = −340 cm^{-1}, ΔE(zero-point energy difference $^6A_1 - {}^2T_2$) = 80 cm^{-1}, c(ratio of vibrational partition functions of the high- and low-spin molecules) = 4.0; FeOH(P-N_4)·$CHCl_3$, high spin, D = 5.3 ± 0.1 cm^{-1}, E = 0.05 ± 0.05 cm^{-1}; FeN_3(P-N_4)·CH_3OH, kinetically controlled spin-crossover, parameters for low-temperature high-spin molecules (22.4%) D = 5 cm^{-1} and E = 0.02 cm^{-1}, low-spin molecules (77.6%) λ = −340 cm^{-1}, Δ = 1320 cm^{-1}, V = 606 cm^{-1}, and κ = 0.83. The solution behavior is more straightforward and resembles that of other 5- or 6-coordinate Fe(III) porphyrins, with respect to UV–visible, ESR, and NMR spectra and ligand binding. The hydroxo complex FeOH(P-N_4) is fully characterized and its properties are compared with those of the closely related μ-oxo oligomer $[Fe(P\text{-}(NO)_4)]_2O$.

Introduction

A correlation between the structural multiformity exhibited by their iron porphyrin centers and the functional diversity of the hemoproteins has been the underlying objective of many of the more recent studies of the chemistry of simpler, well-defined and characterized ferrous and ferric porphyrins. The synthetic analogue approach has been applied successfully to the resolution of fundamental questions concerning the function-related structure of the oxygen carriers hemoglobin and myoglobin,[2] the electron-transporting cytochromes *c*[3] and *c*′,[4] the oxygenase cytochromes P450,[5] and as yet with more limited success to cytochrome oxidase.[6-12]

Our approach[6,7] to a synthetic model for cytochrome oxidase has involved the synthesis of iron porphyrins containing appended ligand systems capable of binding Cu^{2+} ions. The first such system[6] incorporated a tetrapyridine arrangement potentially capable of tetragonal, square-planar, or square-pyramidal coordination to Cu^{2+}. Although we have now shown that this binuclear system has restrictions as a model in that magnetic-exchange coupling between the two metal centers is limited,[6,13,14] interpretation of the physical behavior of these

(1) (a) The Australian National University. (b) Department of Chemistry, Monash University. (c) Department of Physics, Monash University.
(2) Collman, J. P. *Acc. Chem. Res.* **1977**, *10*, 265.
(3) Mashiko, T.; Reed, C. A.; Haller, K. J.; Kastner, M. E.; Scheidt, W. R. *J. Am. Chem. Soc.* **1981**, *103*, 5758.
(4) Reed, C. A.; Mashiko, T.; Bentley, S. P.; Kastner, M. E.; Scheidt, W. R.; Spartalian, K.; Lang, G. *J. Am. Chem. Soc.* **1979**, *101*, 2948.
(5) McCann, S. W.; Wells, F. V.; Wickman, H. H.; Sorrel, T. N.; Collman, J. P. *Inorg. Chem.* **1980**, *19*, 621 and references therein.
(6) Gunter, M. J.; Mander, L. N.; McLaughlin, G. M.; Murray, K. S.; Berry, K. J.; Clark, P. E.; Buckingham, D. A. *J. Am. Chem. Soc.* **1980**, *102*, 1470.
(7) Gunter, M. J.; Mander, L. N.; Murray, K. S.; Clark, P. E. *J. Am. Chem. Soc.* **1981**, *103*, 6784.
(8) (a) Petty, R. H.; Welch, B. R.; Wilson, L. J.; Bottomley, L. A.; Kadish, K. M. *J. Am. Chem. Soc.* **1980**, *102*, 611. (b) Dessens, S. E.; Merrill, C. L.; Saxton, R. J.; Ilaria, R. L., Jr.; Lindsey, J. W.; Wilson, L. J. *Ibid.* **1982**, *104*, 4357.
(9) Landrum, J. T.; Hatano, K.; Scheidt, W. R.; Reed, C. A. *J. Am. Chem. Soc.* **1980**, *102*, 6729.
(10) Okawa, H.; Kanda, W.; Kida, S. *Chem. Lett.* **1980**, 1281.
(11) Jaud, J.; Journaux, Y.; Galy, J.; Kahn, O. *Nouv. J. Chim.* **1980**, *4*, 629.
(12) (a) Chang, C. K. In "Biochemical and Clinical Aspects of Oxygen"; Caughey, W. S., Ed.; Academic Press: New York, 1979; p 437. (b) Chang, C. K.; Koo, M. S.; Ward, B. *J. Chem. Soc., Chem. Commun.* **1982**, 716.
(13) Berry, K. J.; Clark, P. E.; Gunter, M. J.; Murray, K. S. *Nouv. J. Chim.* **1980**, *4*, 581.
(14) Gunter, M. J.; Berry, K. J.; Murray, K. S.; Clark, P. E., manuscript in preparation.

0020-1669/84/1323-0283$01.50/0

complexes has been far from straightforward. At the outset it was clear that ligation of Cu^{2+} by the Fe(III) porphyrin system caused considerable perturbation of the electronic environment on the iron. To interpret the cause and extent of this effect, it was necessary to examine first the physical properties of the Cu-free derivatives. It soon became evident that the mononuclear Fe(III) porphyrin complexes exhibited unusual and complex properties, at least in the solid state. Herein we describe a structure and some of the properties of these complexes, which are of interest in their own right but which also are essential for a full description of the properties of the binuclear systems that are to be reported shortly.[14]

An X-ray structural determination on the chloro–Fe(III) complex of this ligand system reveals a six-coordinate Fe with Cl^- and pyridine (nicotinamide) axial ligands. Such mixed-ligand species have been implicated in the high- to low-spin conversion of Fe(III) porphyrin halides on titration with a strong ligand field axial base, but their presence has been detected only in certain cases; spectroscopic studies have shown the probable existence of the high-spin species Fe(TPP)Cl(*N*-MeIm) (TPP = anion of *meso*-tetraphenylporphyrin, *N*-MeIm = *N*-methylimidazole) in solution,[15] and monoimidazole Fe(III) porphyrins have been synthesized by thermal means, although the products were not fully investigated.[16a] Intermediate-spin monoamine adducts of $Fe(OEP)ClO_4$ have been studied as models for ferricytochrome *c*′.[16b] The only previously determined structure for Fe(III) porphyrins with two different ligands are the low-spin azido(pyridinato)(tetraphenylporphinato)iron(III),[17a] the high- and low-spin Fe(TPP)(py)(NCS) and Fe(OEP)(py)(NCS),[17b] the cytochrome P-450 models of Collman containing thiol and thiolate ligands,[18] and the cytochrome *c* models of Reed and Scheidt.[3] We illustrate that this complex is neither purely high nor low spin in the solid state and as such is of particular interest with regard to the questions or spin-state–structure correlations. Examples of Fe(III) porphyrins in most of the various spin states have now been structurally examined and include five-[19] and six-coordinate $S = {}^5/_2$ high-spin,[20,21] six-coordinate $S = {}^1/_2$ low-spin,[19] $S = {}^3/_2$ intermediate-spin,[22] quantum mixed $S = {}^3/_2, {}^5/_2$ intermediate-spin,[4] and $S = {}^1/_2, S = {}^5/_2$ spin-equilibrium[23] hemes. The present studies provide some insight into the significance of protein influences on heme stereochemistry, such as the variation of spin state and out-of-plane displacement of the Fe(III) atom with the combination of axial igands and doming and core expansion effects of the porphyrin to accommodate an essentially high-spin Fe(III) ion.

Detailed magnetic susceptibility, Mössbauer, and ESR measurements are used to determine the electronic state of the iron and indicate that these complexes are finely balanced near the spin-crossover point. The biological importance of spin-state equilibria in certain hemoproteins has been discussed[24] and has prompted a number of investigations into simpler Fe(III) complexes exhibiting spin-crossover properties. It is evident from solid-state studies that the magnetic properties can be influenced by subtle lattice effects arising from such factors as solvation, intermolecular interactions, and cooperativity effects, as well as from mechanical sample preparation such as grinding and doping into host crystals. A rationalization of these effects has been made in the case of Fe(III) Schiff base complexes,[25] and a quantitative explanation has been advanced for the apparently conflicting arguments regarding the question of quantum-mechanical mixing of spin states–intermediate spin–spin equilibrium in Fe(III) porphyrins.[26] The present complexes also display properties indicative of ground states ($^6A_1$, $^4A_2$, and ^2E) close in energy, and a phenomenological description of the magnetic properties is attempted.

It is now well established that the product obtained on treatment of most Fe(III) porphyrins with base, or on autoxidation of Fe(II) porphyrins, is the μ-oxo oligomer.[27] This is in contrast to certain protein derivatives, for example, metmyoglobin hydroxide, where the hematin hydroxide is formed, since dimerization is sterically prevented. Aqueous solution studies of simpler Fe(III) porphyrins in alkaline media have been at variance, and a uniform picture of the extent and mechanism of aggregation and the involvement of additional hydroxo species has not yet emerged. The isolation and characterization of the hydroxo complex and the μ-oxo oligomer of a closely related derivative of the title Fe(III) porphyrin allows a unique comparison of their properties and ligand binding behavior.

Experimental Section

Compound Preparation. *meso*-α,α,α,α-Tetrakis(*o*-nicotinamidophenyl)porphyrin (P-N_4). A solution of *meso*-α,α,α,α-tetrakis(*o*-aminophenyl)porphyrin[28,29] (3.60 g, 5.34 mmol) in dry dichloromethane (250 mL) was added under N_2 to a stirred solution of nicotinic anhydride (Koch-Light, 25.0 g, 110 mmol) in dichloromethane (250 mL) and pyridine (10 mL). After 36 h at 15 °C, the solution was poured into water (250 mL), the organic layer was separated, and the aqueous layer was extracted with chloroform (2 × 200 mL). After washing ($NaHCO_3$, 2 × 200 mL; H_2O, 100 mL), drying (K_2CO_3), and evaporation of the combined extracts, the residue was stirred 1 h with $NaHCO_3$ solution (5%, 200 mL) and MeOH (50 mL). After filtering, the process was repeated, and the purple solid was washed well with H_2O and dried in vacuo. Recrystallization from chloroform–methanol–hexane gave the hydrate (P-N_4)·H_2O (5.40 g, 93%). TLC ($CHCl_3$–MeOH 9:1): R_f = 0.4. Anal. Calcd for $C_{68}H_{46}N_{12}O_4 \cdot H_2O$: C, 73.36; H, 4.35; N, 15.10. Found: C, 73.27; H, 4.34; N, 14.96. Mass spectrum: m/z 1095 (M^+). λ_{max} ($CHCl_3$): 423, 516, 548, 590, 645 nm.

(15) (a) La Mar, G. N.; Walker, F. A. *J. Am. Chem. Soc.* **1972**, *94*, 8607. (b) Doeff, M. A.; Sweigart, D. A. *Inorg. Chem.* **1982**, *21*, 3699.
(16) (a) Bullard, L.; Panayappan, R. M.; Thorpe, A. N.; Hambright, P. *Bioinorg. Chem.* **1974**, *3*, 161. (b) Ogoshi, H.; Sugimoto, H.; Watamabe, E.; Yoshida, Z.; Maeda, Y.; Sakai, H. *Bull. Chem. Soc. Jpn.* **1981**, *54*, 3414.
(17) (a) Scheidt, W. R. *Acc. Chem. Res.* **1977**, *10*, 343. (b) Scheidt, W. R.; Lee, Y. J.; Geiger, D. K.; Taylor, K.; Hatano, K. *J. Am. Chem. Soc.* **1982**, *104*, 3367.
(18) Collman, J. P.; Sorrell, T. N.; Hodgson, K. O.; Kulshrestha, A. K.; Strouse, C. E. *J. Am. Chem. Soc.* **1977**, *99*, 5180.
(19) (a) Scheidt, W. R. In "The Porphyrins"; Dolphin, D., Ed.; Academic Press: New York, 1979; Vol. III, p 483 ff. (b) Scheidt, W. R. *Acc. Chem. Res.* **1977**, *10*, 339.
(20) (a) Mashiko, T.; Kastner, M. E.; Spartalian, K.; Scheidt, W. R.; Reed, C. A. *J. Am. Chem. Soc.* **1978**, *100*, 6354. (b) Kastner, M. E.; Scheidt, W. R.; Mashiko, T.; Reed, C. A. *Ibid.* **1978**, *100*, 666.
(21) Gans, P.; Buisson, G.; Duee, E.; Regnard, J.-R.; Marchon, J.-C. *J. Chem. Soc., Chem. Commun.* **1979**, 393.
(22) Masuda, H.; Taga, T.; Osaki, K.; Sugimoto, H.; Yoshida, Z.-I.; Ogoshi, H. *Inorg. Chem.* **1980**, *19*, 955.
(23) Scheidt, W. R.; Geiger, D. K. *J. Chem. Soc., Chem. Commun.* **1979**, 1154.
(24) Maltempo, M. M.; Moss, T. H. *Q. Rev. Biophys.* **1976**, *9*, 181.
(25) (a) Haddad, M. S.; Lynch, M. W.; Federer, W. D.; Hendrickson, D. N. *Inorg. Chem.* **1981**, *20*, 123. (b) *Ibid.* **1981**, *20*, 131.
(26) Gregson, A. K. *Inorg. Chem.* **1981**, *20*, 81.
(27) White, W. I. In "The Porphyrins"; Dolphin, D., Ed.; Academic Press: New York, 1979; Vol. V, p 318 ff.
(28) Lindsey, J. *J. Org. Chem.* **1980**, *45*, 5215.
(29) Collman, J. P.; Gagnê, R. R.; Reed, C. A.; Halbert, T. R.; Lang, G.; Robinson, W. T. *J. Am. Chem. Soc.* **1975**, *97*, 1427.
(30) De Meulenauer, J.; Tompa, H. *Acta Crystallogr.* **1965**, *19*, 1014.
(31) Busing, W. R.; Levy, H. A. *J. Chem. Phys.* **1957**, *26*, 563.
(32) Corfield, P. W. R.; Doedens, R. J.; Ibers, J. A. *Inorg. Chem.* **1967**, *6*, 197.
(33) Declerq, J. P.; Germain, G.; Main, P.; Wolfson, M. M. *Acta Crystallogr., Sect. A: Cryst. Phys., Diffr., Theor. Gen. Crystallogr.* **1973**, *A29*, 231.
(34) "International Tables for X-ray Crystallography"; Kynoch Press: Birmingham, 1974; Vol. 4.
(35) Ferguson, J.; Mau, A. W.-H.; Whimp, P. O. *J. Am. Chem. Soc.* **1979**, *101*, 2363.
(36) Johnson, C. K. *Oak Ridge Natl. Lab.* [*Rep.*], *ORNL (U.S.)* **1976**, *ORNL-5138*.

Chloro(*meso*-α,α,α,α-tetrakis(*o*-nicotinamidophenyl)porphinato)iron(III), FeCl(P-N_4). To an argon-flushed solution of (P-N_4) (0.43 g) in acetic acid (100 mL) and pyridine (2.0 mL) was added a saturated aqueous solution of $FeSO_4$ (7 mL). The solution was vigorously stirred and heated at 80 °C for 12 min and then cooled to 25 °C. Air was bubbled through the solution for 3 min and the acetic acid evaporated in vacuo. The residue was partitioned between $CHCl_3$ (60 mL) and H_2O (100 mL). After further extraction with $CHCl_3$ (2 × 60 mL), the organic layers were washed successively with H_2O (2 × 60 mL), 2.5% aqueous NaOH (2 × 60 mL), H_2O (60 mL), 0.05 M HCl (3 × 80 mL), and H_2O (60 mL), dried (Na_2SO_4), and evaporated. After drying at 0.02 mm for 2 h, the solid was recrystallized twice from $CHCl_3$–hexane to give dark lustrous crystals of the chloroform solvate FeCl(P-N_4)·$CHCl_3$ (0.39 g, 76%). TLC ($CHCl_3$–MeOH 9:1): R_f 0.25. Anal. Calcd for $C_{68}H_{44}N_{12}O_4ClFe·CHCl_3$: C, 63.56; H, 3.48; N, 12.89. Found: C, 63.69; H, 3.75; N, 12.70. Quantitative GLC analysis: $CHCl_3$, 0.9 ± 0.2. ESR: solid, g = 9.1, 7.8, 6.5, 5.0, 3.4, 2.0; $CHCl_3$ solution, $g_\perp$ = 5.9, $g_\parallel$ = 2.0.

TLC analysis of the mother liquors from the crystallization revealed the presence of minor amounts of other isomers arising from atropisomerization of the ligand under the conditions of Fe insertion. No trace of these other more soluble isomers was present in the twice-recrystallized product. The integrity of the purified FeCl(P-N_4) was further confirmed by removal of Fe under mild conditions ($FeSO_4$, HOAc, HCl, room temperature, 5 min[37b]) and TLC analysis of the resulting free base porphyrin. This was shown to be homogeneous and free of any other atropisomer. (For comparison, a mixed-isomer preparation was obtained from reaction of a mixture of the four atropisomers of *meso*-tetrakis(*o*-aminophenyl)porphyrin with nicotinic anhydride under conditions similar to those used for the preparation of the α,α,α,α-isomer described above.)

FeBr(P-N_4). This compound was prepared in a manner analogous to that for FeCl(P-N_4), except that the $CHCl_3$ solution of the base-washed reaction mixture was washed with 0.05 M HBr instead of HCl. Recrystallization from $CHCl_3$–toluene gave the chloroform solvate FeBr(P-N_4)·$CHCl_3$. Anal. Calcd for $C_{68}H_{44}N_{12}O_4BrFe·CHCl_3$: C, 61.46; H, 3.36; N, 12.47. Found: C, 61.05; H, 3.43; N, 12.35. Quantitative GLC solvate analysis: $CHCl_3$, 0.93 ± 0.05. ESR: solid, g = 6.1, 2.0; $CHCl_3$ solution, $g_\perp$ = 6.1, $g_\parallel$ = 2.0.

Recrystallization from $CHCl_3$–hexane gave a second sample containing 10% hexane of solution. Anal. Calcd for $C_{68}H_{44}N_{12}O_4BrFe·0.9CHCl_3·0.1C_6H_{14}$: C, 62.06; H, 3.46; N, 12.50. Found: C, 62.25; H, 3.55; N, 12.34. Quantitative GLC solvate analysis: $CHCl_3$, 0.90 ± 0.05; C_6H_{14}, 0.10 ± 0.05.

FeOH(P-N_4). A solution of FeCl(P-N_4) (0.50 g) in $CHCl_3$ (100 mL) was washed with 2.5% aqueous NaOH (3 × 50 mL) and H_2O (100 mL) and dried over Na_2SO_4. Recrystallization ($CHCl_3$–hexane) of the residual solid after evaporation of solvent gave the chloroform solvate FeOH(P-N_4)·$CHCl_3$ as black needles (0.47 g, 95%). Anal. Calcd for $C_{68}H_{45}N_{12}O_5Fe·CHCl_3$: C, 64.47; H, 3.61; N, 13.01; Fe, 4.34. Found: C, 64.30; H, 3.81; N, 12.60; Fe, 4.28. Quantitative GLC analysis for $CHCl_3$: 1.0 ± 0.1. ESR: solid, g = 6.40, 5.12, 4.51, 2.0; Me_2SO solution, $g_\perp$ = 6.0, $g_\parallel$ = 2.0.

FeN_3(P-N_4). An aqueous solution of HN_3 was prepared by passing a saturated aqueous solution of NaN_3 (30 mL) through a column of acidic ion-exchange resin (Bio-Rad AG50W-X8, 25-mL bed volume). A solution of FeOH(P-N_4)·$CHCl_3$ (0.30 g) in $CHCl_3$ (50 mL) was shaken with this solution over 15 min. The organic layer was washed with H_2O (3 × 50 mL), evaporated, and dried in vacuo. The residue was recrystallized from $CHCl_3$–MeOH–hexane to give black crystals of the methanol solvate FeN_3(P-N_4)·CH_3OH (0.21 g, 74%). Anal. Calcd for $C_{68}H_{44}N_{15}O_4Fe·CH_3OH$: C, 67.76; H, 3.96; N, 17.17; Fe, 4.57. Found: C, 67.67; H, 3.96; N, 16.99; Fe, 4.77. ESR: solid, g = 6.10, 2.78, 2.04, 1.95, 1.42; 9:1 $CHCl_3$–MeOH solution, g = 6.00, 2.74, 2.04, 1.94.

[Fe(P-$(NO)_4$)]$_2$O. To a solution of FeOH(P-N_4) (57 mg, 44.4 mol) in Me_2SO (10 mL) was added a solution of trimethylamine *N*-oxide in Me_2SO (0.5 M, 180 μL, 90 μmol). After several days at room temperature, the crystals were filtered off, washed well with methanol, and dried in vacuo; yield 36 mg (63%). Anal. Calcd for $C_{136}H_{88}N_{24}O_{17}Fe_2$: C, 66.89; H, 3.63; N, 13.76; Fe, 4.57. Found: C, 66.91; H, 3.82; N, 13.72; Fe, 4.43.

(37) (a) Smith, K. M., Ed. "Porphyrins and Metalloporphyrins"; Elsevier: New York, 1975; p 803. (b) *Ibid.*, p 800.

Physical Measurements. Variable-temperature bulk magnetic susceptibility measurements were made on an Oxford Instruments Faraday magnetometer, which incorporated a superconducting magnet and automatic data logging facility. Main fields of 10 and 40 kG were used to check any field dependence. A gradient field of 1 kG/cm, calibrated against pure nickel, was used. The temperature was measured with a thermocouple that was calibrated relative to a gallium arsenide diode suspended in the sample position. Samples of about 20 mg mass, contained in a gold bucket, were suspended from a Sartorius microbalance by a fine quartz fiber. Tables of susceptibilities as a function of temperature for the FeX-(P-N_4) complexes are given in the supplementary data (Tables V, VII–IX).

ESR spectra were obtained with a JEOL JES-PE3 X-band spectrometer equipped with an Oxford Instruments helium-flow cryostat. The magnetic field was calibrated with a fixed-frequency oscillator, manual gauss meter, and frequency counter. DPPH was used as a marker.

For Mössbauer spectra a ^{57}Co in Rh source was used, and velocity calibrations were made with a natural α-Fe foil. Isomer shifts are quoted relative to α-Fe.

UV–visible spectra were obtained on a Varian DMS-90 spectrophotometer. The Soret regions of the spectrum were measured with use of a 0.1-mm cell, and the visible bands were measured at the same concentration in a 1.0-mm cell.

Crystal data: $C_{68}H_{44}FeN_{12}O_4·CHCl_3·H_2O$, M_r = 1286.5, monoclinic, $P2_1/c$, a = 14.739 (6) Å, b = 21.924 (7) Å, c = 19.524 (6) Å, β = 101.03 (3)°, V = 6192.4 Å^3, Z = 4, D_m = 1.37, D_c = 1.380 Mg m^{-3}, $F(000)$ = 662, Mo Kα, λ = 0.7107 Å, μ(Mo Kα) = 0.44 mm^{-1}.

Data Collection. Crystals suitable for data collection were obtained by slow recrystallization from $CHCl_3$–hexane. The diffraction symmetry and systematic absences uniquely define the monoclinic space group $P2_1/c$ (C_{2h}^5, No. 14). Diffraction data were collected on a Picker FACS1 automatic four-circle diffractometer using graphite-monochromated Mo Kα radiation. Precise values of the unit cell dimensions and crystal orientation matrix were determined by least-squares analysis of the setting angles of the Mo $K\alpha_1$ (λ = 0.7093 Å) peaks of 12 carefully centered reflections having 2θ values between 33 and 38°. Dimensions of the specimen crystal were 0.044 × 0.042 × 0.020 mm between the bounding faces $(\bar{1}\bar{1}0)$–$(\bar{1}\bar{1}0)$, $(1\bar{1}0)$–$(\bar{1}10)$, and $(0\bar{1}1)$–$(01\bar{1})$, respectively. Reflection intensities were measured in the $\theta/2\theta$ scan mode with a scan velocity (2θ) of 2° min^{-1} and scan width from $2\theta(K\alpha_1)$ − 0.9° to $2\theta(K\alpha_2)$ + 0.9°. Stationary-crystal–stationary-counter backgrounds of 10-s duration were measured at each extreme of the scan width and assumed to vary linearly between these extremes. Intensities of three standard reflections (300, 0,10,0, and 008) were monitored regularly throughout data collection and did not exhibit any significant variations in their intensities during the course of the experiment. Data that were within the range 3° < 2θ(Mo $K\alpha_1$) < 50° and spanned one unique quadrant of reciprocal space ($+h,+k,\pm l$) were collected. Of the 11 753 reflections measured (excluding standards) only 5668 (48%) for which $I > 3\sigma(I)$ were accepted as being significantly above background and, after sorting and averaging of equivalent forms only the unique 5042 reflections were used in the calculations subsequent to structure solution by direct methods. Intensities were corrected for Lorentz, polarization, and absorption effects. Transmission factors for F_0 calculated by the analytical method of De Meulenauer and Tompa[30] varied from 0.954 to 0.965. The statistical residual, R_s ($=\sum\sigma/\sum|F_o|$, where σ is the error contribution to F_o from counting statistics alone), for this data set is 0.041. In the calculation of σ_2 values an experimental uncertainty factor of p = 0.04[31,32] was assumed.

Structure Analysis. Coordinates of most of the non-hydrogen atoms were obtained by use of the direct methods program suite MULTAN.[33] The remainder, which were all associated with one nicotinamide ligand, were obtained after refinement of the atoms already found from electron density difference maps, which also indicated disorder of the $CHCl_3$ molecule. On refinement the thermal parameters of the atoms of this nicotinamide group became very large, consistent with positional disordering presumably due to the loose packing in that part of the structure. In fact, the positional parameters of the terminal atoms of the ligand (isotropic B's ≈ 20) did not undergo sensible refinement and were held at their initially determined values. Several attempts were made to obtain a chemically sensible model for the disordered $CHCl_3$ molecule. One chlorine atom (Cl(4)) could be resolved over two sites, but the others were more diffuse. Again, the carbon atom

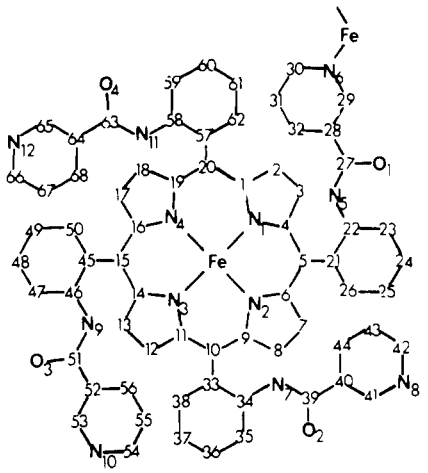

Figure 1. Numbering scheme used for the atoms of a unit of $[FeCl(P\text{-}N_4)]_n$.

and the disordered Cl(4)'s had to be constrained during refinement. The final scattering model was one with anisotropic thermal parameters for the Fe, Cl's (except Cl(4)) and the "floppy" ligand, isotropic thermal parameters for the others, and calculated isotropic hydrogens (except those of H_2O and $CHCl_3$) as fixed-atom contributors. Refinement of this model by full-matrix least squares converged to an R of 0.104 and R_w ($=[\sum w(|F_o| - |F_c|)^2/\sum wF_o^2]^{1/2}$) of 0.122. The function minimized was $\sum w(|F_o| - |F_c|)^2$, where $w = \sigma^{-2}(F)$. Atomic scattering factors together with corrections for anomalous dispersion were taken from ref 34. In the final difference map there were peaks of 0.6–0.8 e Å^{-3} associated with the disorder of the $CHCl_3$ molecule and the "floppy" ligand. Atomic coordinates are listed in Table I, and the atom nomenclature is defined in Figure 1. Tables of observed and calculated structure factor amplitudes are listed in the supplementary material.

Computer Programs. The Picker Corp. FACS-1 disk operating system (1972) was used for diffractometer control and the ANUCRYS structure determination package[35] (P. O. Whimp, D. Taylor, and G. M. McLaughlin) was used in all phases of the structure analysis. The molecular drawing was produced by using the ANUCRYS implementation of ORTEP.[36]

Synthesis and Reactions

An improved procedure[28] for the isolation in high yield of the $\alpha,\alpha,\alpha,\alpha$ isomer of *meso*-tetrakis(*o*-aminophenyl)porphyrin[29] and a straightforward condensation with nicotinic anhydride allow the preparation of the ligand ($P\text{-}N_4$) in gram quantities. The ferrous sulfate–acetic acid method[37a] of iron insertion into the porphyrin avoids any appreciable atropisomerization during the incorporation, and the $FeCl(P\text{-}N_4)$ and $FeBr(P\text{-}N_4)$ complexes can be obtained pure by crystallization. The integrity of the recrystallized product was established by chromatographic comparison of both the $FeCl(P\text{-}N_4)$ complex and the derived free base (obtained by removal of Fe under mild conditions, see Experimental Section) with preparations obtained from a mixed-atropisomer sample of *meso*-tetrakis(*o*-aminophenyl)porphyrin. No trace of the other isomers was detected in the samples used in the present investigation. A small amount of isomerization was evident during the Fe insertion as judged by TLC of the crude reaction mixture and the recrystallization mother liquors. However, the less soluble $\alpha,\alpha,\alpha,\alpha$ isomer readily crystallized from the mixture, or on a smaller scale, purification by chromatography on silica was found convenient. Treatment of a chloroform solution of either the chloro or the bromo compound with aqueous sodium hydroxide solution results in the hematin $FeOH(P\text{-}N_4)$. The hydroxo formulation has been established by a variety of physical methods (see below). This is in contrast to the behavior of simple hemin derivatives, which form μ-oxo oligomers on treatment with base. The reason for this atypical behavior in the present complexes is not obvious. Assuming the chloride

Scheme I

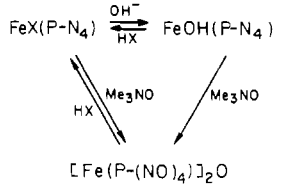

or bromide ions are bound to the iron inside the "pocket" in solution as is the case in the solid state (see Description of the Structure), then displacement by OH^- may occur on the same or opposite side of the porphyrin. If on the same side, the hydroxo ligand may be stabilized inside the pocket by hydrophilic interactions with the NH groups of the amide bonds, although the NH···OH distance is too large to engender any direct hydrogen bonding. If displacement occurs on the opposite side and the OH^- is ligated outside the pocket, then we see no apparent reason why dimerization to the μ-oxo oligomer is disfavored; other "picket-fence"[29] and facially encumbered hemins[38] readily form such oligomers, as does the derived *N*-oxide of this system, which is quite stable in solution or the solid state in the presence of a variety of reagents including aqueous base.

Treatment of solutions of $FeOH(P\text{-}N_4)$ with acids HX (X = Cl, Br, N_3) results in the ready formation of $FeX(P\text{-}N_4)$. Hence, interconversions for various X are possible. The hematin hydroxide is also formed on autoxidation of the Fe(II) derivative, which is available from reduction of the Fe(III) complexes.[39] However, reaction between $FeOH(P\text{-}N_4)$ or $FeX(P\text{-}N_4)$ (X = Cl, Br) and trimethylamine *N*-oxide in Me_2SO solution produces the μ-oxo oligomer of the tetrapyridine *N*-oxide derivative, $[Fe(P\text{-}(NO)_4)]_2O$. Solutions of this complex are stable over long periods and are not affected by protic solvents or aqueous base. Treatment with acids HX again results in the hemins $FeX(P\text{-}N_4)$), however, according to Scheme I. The mechanism for this transformation has not yet been fully elucidated and is under further investigation.

Although some evidence for the existence in solution of Fe(III) porphyrin hydroxo complexes has been presented in the case of the sterically crowded porphyrins *meso*-tetraanthracenylporphyrin[40] and "basket-handle" porphyrins,[38c] until recently the only previously reported isolated mononuclear Fe(III) hydroxo complex with a porphinoid ligand system is of octaethyldi-*tert*-butylporphodimethene.[41] However, it has been well established that certain protein derivatives such as methemoglobin and metmyoglobin in which dimerization is sterically prevented are Fe(III) hydroxo complexes. More recently, the preparation and characterization of several hydroxo Fe(III) porphyrin derivatives have been reported,[42] as have both the hydroxo and μ-oxo complexes in another series of potentially binuclear porphyrin complexes.[7] Until then this compound represented the first reported[39] well-characterized example of a hydroxo Fe(III) porphyrin; analytical, spectroscopic, magnetic, and Möessbauer evidence establishes the hydroxo formulation and allows a comparison with physical data of the μ-oxo oligomer of the closely related tetra-*N*-oxide.

The IR spectrum (mull) of $FeOH(P\text{-}N_4)$ shows bands at 3420 and 3200 cm^{-1} (OH, NH) and lacks any significant

(38) For examples see: (a) Almog, J.; Baldwin, J. E.; Huff, J. *J. Am. Chem. Soc.* **1975**, *97*, 226. (b) Baldwin, J. E.; Klose, T.; Peters, M. *J. Chem. Soc., Chem. Commun.* **1976**, 881. (c) Momenteau, M.; Loock, B.; Mispelter, J.; Bisagni, E. *Nouv. J. Chim.* **1979**, *3*, 77.
(39) Gunter, M. J.; Mander, L. N.; Murray, K. S. *J. Chem. Soc., Chem. Commun.* **1981**, 799.
(40) Cense, J.-M.; Le Quan, R.-M. *Tetrahedron Lett.* **1979**, 3725.
(41) Buchler, J. W. *Angew. Chem., Int. Ed. Engl.* **1978**, *17*, 407.
(42) Cheng, R.-J.; Latos-Grazynski, L.; Balch, A. L. *Inorg. Chem.* **1982**, *21*, 2412.

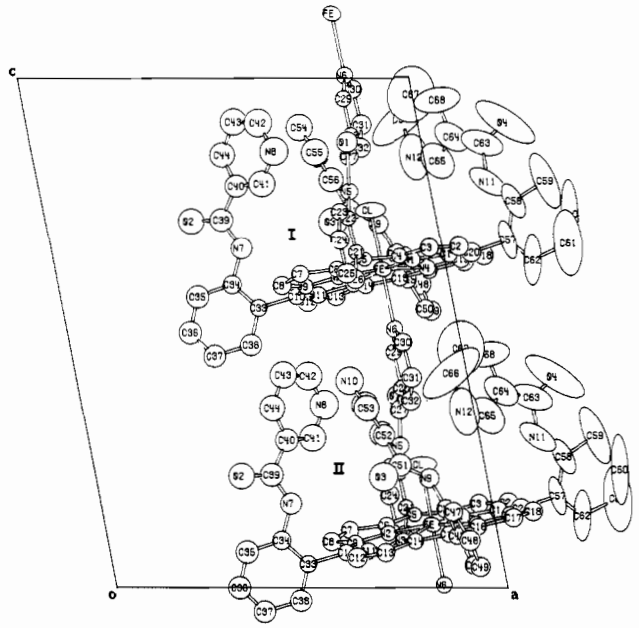

Figure 2. Projection of two of the molecules of $[FeCl(P\text{-}N_4)]_n$ in the unit cell onto the *ac* plane. I is the base molecule with coordinates listed in Table I. II is related to I by the *c* glide $(x, {}^1/_2 - y, z - {}^1/_2)$. The thermal ellipsoid surfaces are scaled to 50% probability. The $CHCl_3$, water molecule, and hydrogen atom positions are omitted for clarity. The polymeric nature of the structure is readily seen as an infinite chain of molecules along *c* with Fe of molecule I bonding to N(6) of molecule II and Fe of molecule II bonding to N(6) of molecule I in the next cell.

bands between 820 and 1000 cm^{-1}; the Fe–O–Fe antisymmetric stretching vibration of all previously reported μ-oxo oligomers appears in the region 850–900 cm^{-1} [27] and for $[Fe(P\text{-}(NO)_4)]_2O$ at 870 cm^{-1}. The magnetic moment measured in solution ($CHCl_3$ or Me_2SO) or the solid state at 300 K is 5.9 μ_B, consistent with high-spin Fe(III) ($S = {}^5/_2$); the moment of the μ-oxo oligomer at 300 K is 2.7 μ_B/Fe in the solid state and 2.2 μ_B/Fe in $CHCl_3$ solution, which although slightly higher than the usual range of 1.6–1.9 μ_B [27] is consistent with strong antiferromagnetic coupling between the two high-spin Fe(III) ions via the oxo bridge. (The higher value may reflect some high-spin Fe(III) impurity, as detected in the ESR spectrum.) The ESR spectrum of the hematin in the solid state or frozen solution ($CHCl_3$ or Me_2SO) at 4.2 K shows $g_\perp \approx 6$ and $g_\parallel \approx 2$ signals typical of high-spin Fe(III) porphyrins; at 4.2 K a frozen-solution ($CHCl_3$) spectrum of the oligomer shows similar signals, but of only ~3% of the intensity of those of the hydroxo complex at the same concentration, and presumably arises from a small amount of a high-spin impurity. The UV–visible spectral and ligand binding differences are discussed below, as are the more detailed magnetic and Möessbauer properties of the hydroxo complex.

Description of the Structure

Tables II and III give the individual bond distances and angles for the $FeCl(P\text{-}N_4)$ molecule. The numbering scheme used is illustrated in the computer-drawn model displayed in Figure 2 and also represented in Figure 1.

Figure 2 clearly shows the polymeric nature of the complex, consisting of infinite chains of $FeCl(P\text{-}N_4)$ units, with a pyridine N of a nicotinamide "picket" of one unit coordinated to the Fe atom of another. The chloride ion of each unit is located inside the "pocket" and completes the six-coordinate arrangement around each Fe. Solvate molecules of chloroform occupy interstices in the crystal lattice, but for clarity they are not included in the figure.

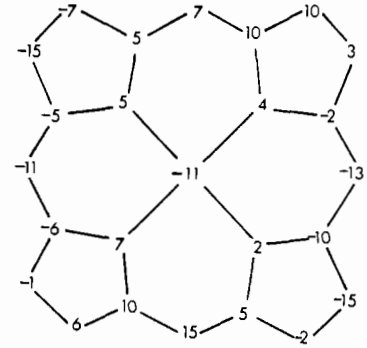

Figure 3. Formal diagram of the porphinato core of a unit of $[FeCl(P\text{-}N_4)]_n$, indicating the perpendicular displacements, in units of 0.01 Å, from the mean plane of the 24-atom core and illustrating the extent of ruffling. The core has the same relative orientation as Figure 2. The standard errors of the displacements are 0.01 Å for C and N atoms and 0.001 Å for Fe.

The Fe atom is displaced moderately (0.138 (1) Å) from the least-squares plane of the four porphinato nitrogen atoms and 0.109 (1) Å from the mean plane of the 24-atom porphyrin core, toward the chloride ion. The average $Fe\text{–}N_{porph}$ distance is 2.042 (8) Å, substantially larger than the 1.990-Å value expected for low-spin six-coordinate iron(III) porphyrins.[19] Similar $Fe\text{–}N_{porph}$ distances of 2.041 (8), 2.045 (5), and 2.03 (1) Å are found for the high-spin six-coordinate complex ions $[Fe(H_2O)_2TPP]^+$,[20b] $[Fe(TMSO)_2TPP]^+$,[20a] and $[Fe(EtOH)_2TPP]^+$,[21] respectively, where the Fe is in the plane of the porphyrin in each case, which are indicative of an occupied or partly occupied $3d_{x^2-y^2}$ orbital on Fe. Typically, five-coordinate high-spin Fe(III) porphyrins have the Fe atom displaced ~0.5 Å from the plane of the core and $Fe\text{–}N_{porph}$ distances of 2.07 Å.[19] Thus, some radial expansion, doming, or ruffling of the porphyrin core is expected in $FeCl(P\text{-}N_4)$ to accommodate the iron atom, which exhibits at least some high-spin character (see below).

However, analysis of the structural data in a manner analogous to that described in ref 19 reveals no significant expansion or contraction of the core. Likewise, it is apparent that doming of the core, which has nonetheless been shown to be an inefficient means of relieving strain for nonexpanded cores, is not an important factor in this case; indeed, the separation of the mean plane of the porphinato N atoms from the mean plane of the porphyrin skeleton is only 0.029 Å and is away from the Fe (i.e., the Fe lies on the *concave* side of the shallow dome). Thus, in the absence of a significant degree of radial core expansion or doming, it is apparent that the principal mechanism by which an essentially high-spin Fe atom can be accommodated is by a deformation of the porphyrin skeleton by an S_4 ruffling. This is most clearly evidenced by the displacement of the C_m carbon atoms alternatively above and below the mean plane of the porphyrin, as illustrated in Figure 3. These results are in contrast to those of the hemins $[Fe(H_2O)_2TPP]^+$[20b] and $[Fe(TMSO)_2TPP]^+$,[20a] which exhibit significant radial expansion of the core in order to accommodate the in-plane high-spin Fe(III) atom, with minimal ruffling of the porphyrin skeleton. Likewise in Fe(OEP)(py)(NCS)[17b] (vide infra) the high-spin Fe atom is accommodated by a combination of core expansion and displacement of the Fe atom from the mean plane of the core.

The dihedral angles between the *meso*-phenyl groups and the mean porphyrin plane are 95.3, 89.1, 75.5, and 85.0° and between the pyridine rings and these phenyl groups are 3.1, 146.3, 8.2, and 145°, respectively.

One of the nicotinamide groups not involved in coordination to a second molecule in the chain exhibits positional disordering associated with loose packing in that section of the structure, as detailed in the Experimental Section. The pyridine ring

Table I. Positional and Thermal Parameters for $Fe(P)Cl(N_4)\cdot CHCl_3\cdot H_2O$

atom	*x/a*	*y/b*	*z/c*	atom	*x/a*	*y/b*	*z/c*
Fe	0.83642 (11)	0.80836 (6)	0.62336 (7)	C(60)	1.3425 (27)	0.7422 (18)	0.7308 (45)
Cl	0.8381 (3)	0.8255 (1)	0.7404 (1)	C(61)	1.3231 (34)	0.7260 (15)	0.6744 (38)
Cl(2)	0.4336 (5)	0.1386 (3)	0.6937 (4)	C(62)	1.2242 (14)	0.7474 (7)	0.6409 (15)
Cl(3)	0.4913 (5)	0.0427 (4)	0.7856 (4)	C(63)	1.1545 (24)	0.8256 (9)	0.8722 (11)
O(4)	1.2238 (18)	0.8161 (7)	0.9126 (11)	C(64)	1.0799 (18)	0.8693 (11)	0.8843 (11)
N(11)	1.1494 (13)	0.8038 (8)	0.7951 (9)	C(65)	1.0322 (17)	0.9125 (11)	0.8365 (13)
N(12)	0.9748	0.9578	0.8439	c(66)	0.9600	0.9575	0.9187
C(57)	1.1711 (11)	0.7683 (7)	0.6804 (13)	C(67)	0.9972	0.9178	0.9666
C(58)	1.2060 (13)	0.7755 (7)	0.7569 (14)	C(68)	1.0605	0.8826	0.9556
C(59)	1.2963 (19)	0.7613 (11)	0.7969 (20)	C(69)	0.4996	0.0738	0.7012

atom	β_{11}	β_{22}	β_{33}	β_{12}	β_{13}	β_{23}
Fe	0.00442 (10)	0.00118 (3)	0.00174 (4)	0.00009 (5)	0.00010 (5)	0.00018 (3)
Cl	0.0129 (3)	0.0022 (1)	0.0020 (1)	−0.0002 (1)	0.0010 (1)	0.0001 (1)
Cl(2)	0.0139 (5)	0.0068 (2)	0.0158 (5)	0.0009 (3)	0.0064 (4)	−0.0012 (3)
Cl(3)	0.0160 (6)	0.0122 (4)	0.0135 (4)	0.0006 (4)	0.0027 (4)	0.0031 (3)
O(4)	0.0379 (31)	0.0054 (5)	0.0143 (12)	−0.0042 (10)	−0.0161 (17)	0.0027 (7)
N(11)	0.0147 (17)	0.0041 (5)	0.0065 (8)	−0.0044 (8)	−0.0048 (9)	0.0027 (5)
N(12)	0.0112 (16)	0.0053 (6)	0.0176 (16)	0.0002 (8)	0.0018 (13)	−0.0016 (8)
C(57)	0.0030 (10)	0.0019 (4)	0.0115 (12)	−0.0010 (5)	−0.0009 (9)	0.0019 (5)
C(58)	0.0058 (13)	0.0020 (4)	0.0095 (12)	−0.0004 (6)	−0.0027 (10)	0.0009 (5)
C(59)	0.0083 (19)	0.0042 (8)	0.0251 (30)	−0.0022 (10)	−0.0058 (19)	0.0069 (14)
C(60)	0.0050 (19)	0.0029 (11)	0.0392 (71)	−0.0005 (10)	0.0074 (30)	0.0001 (18)
C(61)	0.0113 (32)	0.0009 (6)	0.0346 (54)	−0.0009 (10)	0.0049 (29)	−0.0006 (12)
C(62)	0.0053 (13)	0.0019 (4)	0.0208 (20)	0.0004 (6)	0.0051 (13)	0.0007 (7)
C(63)	0.0220 (92)	0.0029 (6)	0.0053 (8)	−0.0041 (11)	−0.0030 (12)	0.0006 (6)
C(64)	0.0138 (21)	0.0043 (7)	0.0069 (10)	−0.0043 (10)	−0.0025 (12)	0.0015 (7)
C(65)	0.0138 (22)	0.0057 (8)	0.0103 (12)	−0.0014 (11)	−0.0011 (13)	−0.0010 (8)
C(66)	0.0552 (82)	0.0200 (28)	0.0204 (29)	−0.0103 (37)	0.0263 (41)	−0.0130 (25)
C(67)	0.0313 (55)	0.0199 (29)	0.0244 (37)	−0.0150 (34)	0.0069 (36)	−0.0074 (28)
C(68)	0.0303 (42)	0.0128 (16)	0.0050 (9)	−0.0134 (23)	0.0041 (15)	−0.0022 (9)
C(69)	0.0353 (44)	0.0161 (18)	0.0043 (8)	0.0046 (12)	0.0047 (15)	−0.0005 (10)

atom	U_{11}	U_{22}	U_{33}	U_{12}	U_{13}	U_{23}
Fe	0.0468 (10)	0.0287 (7)	0.0325 (8)	0.0015 (8)	0.0014 (7)	0.0039 (7)
Cl	0.137 (3)	0.054 (2)	0.037 (2)	−0.004 (2)	0.0014 (2)	0.002 (1)
Cl(2)	0.148 (6)	0.166 (5)	0.294 (9)	0.0014 (5)	0.090 (6)	−0.025 (5)
Cl(3)	0.170 (7)	0.298 (9)	0.252 (8)	0.009 (7)	0.038 (6)	0.066 (7)
O(4)	0.402 (32)	0.131 (13)	0.267 (22)	−0.067 (16)	−0.226 (24)	0.057 (14)
N(11)	0.156 (18)	0.100 (12)	0.121 (14)	−0.071 (12)	−0.067 (12)	0.057 (11)
N(12)	0.119 (17)	0.130 (15)	0.327 (30)	0.004 (13)	0.026 (18)	−0.034 (17)
C(57)	0.031 (10)	0.047 (9)	0.214 (21)	−0.015 (8)	−0.012 (12)	0.040 (11)
C(58)	0.061 (14)	0.048 (10)	0.177 (22)	−0.006 (9)	−0.038 (14)	0.019 (11)
C(59)	0.088 (20)	0.102 (19)	0.468 (56)	−0.035 (16)	−0.082 (26)	0.148 (29)
C(60)	0.054 (20)	0.070 (28)	0.730 (131)	−0.008 (16)	0.103 (43)	0.002 (39)
C(61)	0.120 (34)	0.022 (13)	0.644 (100)	−0.015 (15)	0.069 (41)	−0.012 (27)
C(62)	0.056 (14)	0.045 (10)	0.387 (36)	0.007 (10)	0.071 (18)	0.015 (14)
C(63)	0.233 (30)	0.071 (13)	0.099 (15)	−0.066 (17)	−0.042 (17)	0.012 (12)
C(64)	0.146 (22)	0.104 (16)	0.128 (18)	−0.069 (15)	−0.036 (17)	0.032 (14)
C(65)	0.147 (24)	0.139 (20)	0.192 (23)	−0.023 (17)	−0.016 (19)	−0.022 (18)
C(66)	0.585 (87)	0.487 (67)	0.380 (54)	−0.166 (59)	0.370 (58)	−0.277 (53)
C(67)	0.332 (58)	0.484 (71)	0.454 (69)	−0.241 (55)	0.096 (51)	−0.157 (59)
C(68)	0.321 (45)	0.312 (38)	0.094 (17)	−0.215 (36)	0.057 (22)	−0.047 (20)
C(69)	0.374 (46)	0.392 (44)	0.079 (15)	0.074 (36)	0.065 (21)	−0.011 (21)

atom	*x/a*	*y/b*	*z/c*	*B*, Å²	atom	*x/a*	*y/b*	*z/c*	*B*, Å²
Cl(4A)	0.4397	0.0294	0.6309	15.4 (4)	C(42)	0.5941 (13)	0.8068 (8)	0.9137 (9)	9.0 (4)
Cl(4B)	0.5220	0.0254	0.655	17.4 (5)	C(43)	0.5315 (12)	0.8487 (7)	0.1958 (8)	8.2 (4)
O(1)	0.8126 (6)	0.5566 (3)	0.8761 (4)	5.0 (2)	C(44)	0.4873 (11)	0.8707 (7)	0.8511 (8)	7.4 (4)
O(2)	0.3738 (8)	0.8912 (4)	0.7182 (5)	7.7 (2)	C(45)	0.8952 (7)	1.0296 (4)	0.6015 (5)	3.4 (2)
O(3)	0.7364 (8)	1.1078 (5)	0.7174 (6)	9.6 (3)	C(46)	0.8795 (8)	1.0669 (5)	0.6544 (5)	4.0 (2)
O(5)	0.6248 (14)	0.1357 (9)	0.9812 (10)	20.8 (7)	C(47)	0.8968 (8)	1.1303 (5)	0.6484 (6)	4.3 (2)
N(1)	0.9170 (6)	0.7318 (3)	0.6407 (4)	2.9 (2)	C(48)	0.9263 (9)	1.1511 (5)	0.5927 (6)	4.9 (3)
N(2)	0.7213 (6)	0.7541 (3)	0.6074 (4)	2.8 (2)	C(49)	0.9400 (8)	1.1162 (5)	0.5409 (6)	4.5 (3)
N(3)	0.7548 (6)	0.8824 (3)	0.5925 (4)	2.5 (2)	C(50)	0.9250 (8)	1.0524 (5)	0.5446 (5)	4.1 (2)
N(4)	0.9512 (6)	0.8600 (3)	0.6249 (4)	3.1 (2)	C(51)	0.7836 (10)	1.0623 (6)	0.7394 (7)	5.9 (3)
N(5)	0.7935 (6)	0.6130 (4)	0.7775 (4)	3.4 (2)	C(52)	0.7574 (9)	1.0290 (6)	0.7985 (6)	5.3 (3)
N(6)	0.8379 (6)	0.7052 (3)	1.0052 (4)	3.1 (2)	C(53)	0.7277 (11)	1.0612 (7)	0.8515 (8)	7.4 (4)
N(7)	0.4872 (7)	0.8558 (4)	0.6647 (5)	5.3 (2)	C(54)	0.6975 (11)	0.9752 (8)	0.9048 (8)	8.0 (4)
N(8)	0.6216 (10)	0.7814 (6)	0.8579 (8)	9.5 (4)	C(55)	0.7255 (12)	0.9385 (7)	0.8564 (9)	8.5 (4)
N(9)	0.8515 (7)	1.0421 (4)	0.7139 (5)	4.4 (2)	C(56)	0.7529 (10)	0.9662 (7)	0.8014 (7)	6.9 (3)
N(10)	0.6978 (9)	1.0351 (6)	0.9044 (7)	8.8 (3)	H(2)	1.105	0.654	0.677	3.9
C(1)	1.0132 (8)	0.7308 (5)	0.6529 (5)	3.5 (2)	H(3)	0.965	0.591	0.672	3.7
C(2)	1.0422 (8)	0.6689 (5)	0.6675 (5)	4.3 (2)	H(7)	0.603	0.633	0.621	3.7
C(3)	0.9664 (8)	0.6340 (5)	0.6651 (5)	3.9 (2)	H(8)	0.504	0.723	0.578	4.2
C(4)	0.8860 (7)	0.6721 (4)	0.6484 (5)	2.7 (2)	H(12)	0.568	0.960	0.545	4.6
C(5)	0.7960 (7)	0.6544 (4)	0.6429 (4)	2.4 (2)	H(13)	0.709	1.024	0.567	4.4

Table I (*Continued*)

atom	x/a	y/b	z/c	B, Å²	atom	x/a	y/b	z/c	B, Å²
C(6)	0.7205 (7)	0.6919 (4)	0.6232 (5)	3.0 (2)	H(17)	1.071	0.984	0.634	3.8
C(7)	0.6247 (8)	0.6730 (4)	0.6138 (5)	3.5 (2)	H(18)	1.168	0.892	0.663	4.1
C(8)	0.5726 (8)	0.7217 (5)	0.5909 (5)	4.0 (2)	H(23)	0.757	0.495	0.782	3.5
C(9)	0.6323 (7)	0.7723 (4)	0.5887 (5)	2.7 (2)	H(24)	0.732	0.426	0.692	4.3
C(10)	0.6046 (7)	0.8325 (4)	0.5694 (5)	3.1 (2)	H(25)	0.737	0.456	0.580	5.0
C(11)	0.6609 (8)	0.8823 (4)	0.5726 (5)	3.2 (2)	H(26)	0.759	0.561	0.554	4.5
C(12)	0.6300 (9)	0.9460 (5)	0.5594 (6)	4.6 (3)	H(29)	0.816	0.618	0.979	3.1
C(13)	0.7053 (8)	0.9801 (5)	0.5697 (5)	4.0 (2)	H(30)	0.862	0.794	1.011	4.0
C(14)	0.7857 (7)	0.9420 (4)	0.5909 (5)	3.0 (2)	H(31)	0.869	0.807	0.893	4.9
C(15)	0.8757 (8)	0.9608 (4)	0.6049 (5)	3.2 (2)	H(32)	0.846	0.726	0.817	4.6
C(16)	0.9536 (8)	0.9237 (4)	0.6200 (5)	3.3 (2)	H(35)	0.314	0.880	0.602	5.7
C(17)	1.0481 (8)	0.9421 (5)	0.6374 (5)	4.0 (2)	H(36)	0.252	0.870	0.486	5.8
C(18)	1.1014 (8)	0.8929 (5)	0.6499 (5)	4.2 (2)	H(37)	0.339	0.845	0.406	5.3
C(19)	1.0414 (8)	0.8412 (5)	0.6425 (5)	3.6 (2)	H(38)	0.504	0.832	0.442	5.6
C(20)	1.0715 (9)	0.7812 (5)	0.6559 (6)	4.4 (3)	H(41)	0.598	0.789	0.756	7.3
C(21)	0.7784 (7)	0.5896 (4)	0.6570 (5)	2.7 (2)	H(42)	0.633	0.788	0.953	9.9
C(22)	0.7771 (7)	0.5691 (4)	0.7247 (5)	2.7 (2)	H(44)	0.435	0.897	0.850	7.4
C(23)	0.7588 (7)	0.5084 (4)	0.7370 (5)	3.4 (2)	H(47)	0.885	1.158	0.686	4.6
C(24)	0.7427 (8)	0.4678 (5)	0.6814 (5)	4.1 (2)	H(48)	0.938	1.194	0.592	4.8
C(25)	0.7437 (8)	0.4855 (5)	0.6151 (6)	4.7 (3)	H(49)	0.965	1.134	0.502	4.5
C(26)	0.7630 (8)	0.5464 (5)	0.6032 (5)	4.3 (2)	H(50)	0.935	1.025	0.508	3.8
C(27)	0.8103 (8)	0.6071 (5)	0.8476 (5)	3.9 (2)	H(53)	0.736	1.106	0.851	7.2
C(28)	0.8252 (7)	0.6631 (4)	0.8897 (5)	2.7 (2)	H(54)	0.675	0.955	0.946	8.8
C(29)	0.8242 (7)	0.6584 (4)	0.9604 (5)	3.0 (2)	H(55)	0.723	0.894	0.860	9.3
C(30)	0.8523 (8)	0.7597 (5)	0.9789 (5)	3.7 (2)	H(56)	0.777	0.941	0.768	6.9
C(31)	0.8569 (8)	0.7690 (5)	0.9099 (6)	4.6 (3)	H(59)	1.317	0.768	0.851	20.0
C(32)	0.8442 (8)	0.7191 (5)	0.8649 (6)	4.4 (3)	H(60)	1.406	0.733	0.754	17.9
C(33)	0.5018 (8)	0.8433 (4)	0.5469 (5)	3.4 (2)	H(61)	1.364	0.709	0.641	18.7
C(34)	0.4455 (8)	0.8572 (5)	0.5927 (6)	4.0 (2)	H(62)	1.199	0.744	0.588	15.1
C(35)	0.3513 (10)	0.8693 (6)	0.5699 (7)	5.9 (3)	H(65)	1.048	0.911	0.787	13.6
C(36)	0.3145 (10)	0.8634 (6)	0.4994 (7)	6.0 (3)	H(66)	0.921	0.988	0.932	20.0
C(37)	0.3653 (10)	0.8494 (6)	0.4524 (6)	5.7 (3)	H(68)	1.098	0.863	0.994	14.3
C(38)	0.4635 (9)	0.8391 (5)	0.4742 (6)	5.5 (3)	H(N5)	0.795	0.657	0.762	3.9
C(39)	0.4518 (11)	0.8681 (6)	0.7208 (7)	6.2 (3)	H(N7)	0.555	0.849	0.673	5.1
C(40)	0.5076 (10)	0.8479 (6)	0.7888 (7)	6.0 (3)	H(N9)	0.887	1.008	0.736	4.5
C(41)	0.5742 (12)	0.8041 (7)	0.7931 (8)	8.2 (4)	H(N11)	1.085	0.811	0.769	11.3

of this group and that of the group trans to it with respect to the porphyrin are oriented with the N's directed toward the center of the molecule, whereas the pyridine ring involved in coordination to the Fe and its transversely situated partner have the N's directed outward. (Note that solution NMR measurements of the free base porphyrin indicate a conformation with all N's directed away from the center.)[43] The coordinated pyridine is nearly perpendicular to the mean porphyrin core (92.2°), and the N_{py}–Fe–Cl angle is 181.0°. However, the orientation of this ligand is somewhat unfavorable, and the angle ϕ (defined as the dihedral angle between the plane of the ligand and the plane enclosed by N_1–Fe–N_{py})[19] of 24° gives rise to close contacts between the ortho hydrogens of the pyridine and the porphinato atoms N_1 and N_3 of 2.58 and 2.54 Å, respectively. Although these values are close to the sum of the currently accepted van der Waals radii of 2.20 Å (H, 1.0 Å;[44] N, 1.5 Å) they do not necessarily solely account for the long Fe–N_{py} distance of 2.330 (8) Å. Until recently the only reported structure of an Fe(III) porphyrin with inequivalent nitrogen axial ligands was the low-spin derivative Fe(TPP)(N_3)(py);[17a] the Fe–N_{py} distance of 2.085 (6) Å is similar to that of other low-spin six-coordinate Fe porphyrins with two identical axial nitrogen ligands, e.g. (Fe(TPP)-$(Im)_2)^+Cl^-$, with Fe–N_{Im} = 1.957 (4), 1.9991 (5) Å[45] and (Fe(ProtoIX)$(Im)_2)^+$, with Fe–N_{Im} = 1.988 (5), 1.966 (5) Å.[46] Single occupancy of the $3d_{z^2}$ orbital results in a lengthening of the axial bonds;[47,48] this has been demonstrated recently by the structural determination[17b] of two Fe porphyrins having identical axial ligands but exhibiting different spin states, viz., low-spin Fe(TPP)(py)(NCS) and high-spin Fe(OEP)(py)-(NCS). A lengthening of the Fe–N_{py} bond length from 2.082 to 2.442 Å and an increase in the Fe–NCS bond length (1.942 to 2.031 Å) are observed in comparing the low-spin to the high-spin complex. Likewise, the Fe is displaced from the mean plane of the porphyrin toward the NCS ligand in both cases (0.05 and 0.24 Å), and the asymmetry in axial binding is manifest in the different axial bond lengths. Hence in the present structure the Fe–N_{py} bond, although somewhat weak, is indicative of a high- or intermediate-spin state on Fe.

The axial Fe–Cl bond distance of 2.31 (3) Å is longer than those of other high-spin five-coordinate hemin chlorides such as Fe(TPP)(Cl), Fe–Cl = 2.192 (12) Å,[49] and Fe(ProtoIXDME)(Cl), Fe–Cl = 2.218 (6) Å.[50] In these cases it has been suggested[19] that nonbonded interactions between the chloride ion and the porphyrin skeleton, rather than the size of the high-spin Fe atom, are responsible for the out-of-plane displacement of the Fe.[51,52] However, in the present case, the

(43) Buckingham, D. A.; Gunter, M. J.; Mander, L. N. *J. Am. Chem. Soc.* **1978**, *100*, 2899.
(44) Bauer, W. H. *Acta Crystallogr., Sect. B: Struct. Crystallogr. Cryst. Chem.* **1972**, *B28*, 1456.
(45) Collins, D. M.; Countryman, R.; Hoard, J. L. *J. Am. Chem. Soc.* **1972**, *94*, 2066.
(46) Little, R. G.; Dymock, K. R.; Ibers, J. A. *J. Am. Chem. Soc.* **1975**, *97*, 4532.
(47) For example, an increase of 0.4 Å in the axial bond length is observed in the low-spin d^7 Co(II) porphyrin $(Pip)_2$Co(TPP) (Pip = piperidine) compared to that in the corresponding low-spin d^6 Co(III) derivative $(Pip)_2CoTPP^+$[48] as a direct result of population of the d_{z^2} orbital. Scheidt, W. R. *J. Am. Chem. Soc.* **1974**, *96*, 84.
(48) Scheidt, W. R.; Cunningham, J. A.; Hoard, J. L. *J. Am. Chem. Soc.* **1973**, *95*, 8289.
(49) Hoard, J. L.; Cohen, G. H.; Glick, M. D. *J. Am. Chem. Soc.* **1967**, *89*, 1992.
(50) Koenig, D. F. *Acta Crystallogr.* **1965**, *18*, 663.
(51) A similar rationale has been suggested to account for the long Mn–Cl bond, 2.468 (1) Å, and the displacement of 0.12 Å toward the Cl^- of the Mn atom from the porphyrin nitrogen plane in Mn(TPP)(Cl)(py), where the Mn–Cl bond distance has increased by 0.1 Å relative to the five-coordinate Mn(TPP)Cl,[52] and the axial Mn–N_{py} bond, 2.444 (4) Å, is also weak. Kirner, J. F.; Scheidt, W. R. *Inorg. Chem.* **1975**, *14*, 2081.

Table II. Interatomic (Non-Hydrogen) Distances (A)[a]

atoms	dist	atoms	dist	atoms	dist	atoms	dist
Fe-Cl(1)	2.311 (3)	Fe-N(6)	2.330 (8)				
Fe-N(1)	2.047 (8)	Fe-N(2)	2.047 (8)	Fe-N(3)	2.041 (7)	Fe-N(4)	2.031 (9)
N(1)-C(1)	1.39 (1)	N(2)-C(6)	1.40 (1)	N(3)-C(11)	1.36 (1)	N(4)-C(16)	1.40 (1)
N(1)-C(4)	1.40 (1)	N(2)-C(9)	1.35 (1)	N(3)-C(14)	1.39 (1)	N(4)-C(19)	1.37 (1)
C(1)-C(2)	1.43 (1)	C(6)-C(7)	1.45 (1)	C(11)-C(12)	1.48 (1)	C(16)-C(17)	1.43 (2)
C(2)-C(3)	1.35 (1)	C(7)-C(8)	1.34 (1)	C(12)-C(13)	1.32 (2)	C(17)-C(18)	1.33 (2)
C(3)-C(4)	1.44 (1)	C(8)-C(9)	1.42 (1)	C(13)-C(14)	1.44 (2)	C(18)-C(19)	1.43 (2)
C(4)-C(5)	1.37 (1)	C(9)-C(10)	1.41 (1)	C(14)-C(15)	1.37 (2)	C(19)-C(20)	1.40 (2)
C(5)-C(6)	1.38 (1)	C(10)-C(11)	1.37 (1)	C(15)-C(16)	1.39 (1)	C(20)-C(1)	1.39 (2)
C(5)-C(21)	1.48 (1)	C(10)-C(33)	1.51 (1)	C(15)-C(45)	1.54 (1)	C(20)-C(57)	1.48 (2)
C(21)-C(22)	1.40 (1)	C(33)-C(34)	1.37 (2)	C(45)-C(46)	1.37 (2)	C(57)-C(58)	1.49 (3)
C(22)-C(23)	1.39 (1)	C(34)-C(35)	1.40 (2)	C(46)-C(47)	1.42 (2)	C(58)-C(59)	1.44 (3)
C(23)-C(24)	1.39 (1)	C(35)-C(36)	1.39 (2)	C(47)-C(48)	1.33 (2)	C(59)-C(60)	1.63 (9)
C(24)-C(25)	1.35 (1)	C(36)-C(37)	1.33 (2)	C(48)-C(49)	1.31 (2)	C(60)-C(61)	1.14 (10)
C(25)-C(26)	1.39 (2)	C(37)-C(38)	1.45 (2)	C(49)-C(50)	1.42 (2)	C(61)-C(62)	1.55 (5)
C(26)-C(21)	1.40 (1)	C(38)-C(33)	1.43 (2)	C(50)-C(45)	1.37 (2)	C(62)-C(57)	1.28 (3)
C(22)-N(5)	1.40 (1)	C(34)-N(7)	1.42 (1)	C(46)-N(9)	1.41 (1)	C(58)-N(11)	1.37 (3)
N(5)-C(27)	1.35 (1)	N(7)-C(39)	1.33 (2)	N(9)-C(51)	1.28 (2)	N(11)-C(63)	1.57 (3)
C(27)-O(1)	1.24 (1)	C(39)-O(2)	1.25 (2)	C(51)-O(3)	1.24 (2)	C(63)-O(4)	1.18 (4)
C(27)-C(28)	1.47 (1)	C(39)-C(40)	1.49 (2)	C(51)-C(52)	1.48 (2)	C(63)-C(64)	1.51 (4)
C(28)-C(29)	1.39 (1)	C(40)-C(41)	1.36 (2)	C(52)-C(53)	1.39 (2)	C(64)-C(65)	1.42 (3)
C(29)-N(6)	1.34 (1)	C(41)-N(8)	1.41 (2)	C(53)-N(10)	1.33 (2)	C(65)-N(12)*	1.33
N(6)-C(30)	1.33 (1)	N(8)-C(42)	1.35 (2)	N(10)-C(54)	1.31 (2)	N(12)*-C(66)*	1.52
C(30)-C(31)	1.38 (2)	C(42)-C(43)	1.31 (3)	C(54)-C(55)	1.36 (2)	C(66)*-C(67)*	1.32
C(31)-C(32)	1.39 (2)	C(43)-C(44)	1.39 (2)	C(55)-C(56)	1.36 (2)	C(67)*-C(68)*	1.26
C(32)-C(28)	1.37 (1)	C(44)-C(40)	1.40 (2)	C(56)-C(52)	1.38 (2)	C(68)*-C(64)	1.50
C(69)*-Cl(2)	1.71	C(69)*-Cl(3)	1.80	C(69)*-Cl(4a)*	1.77	C(69)*-Cl(4b)*	1.47

[a] Atoms marked with an asterisk were ill-defined and did not undergo sensible refinement. Their positional parameters were therefore held at their initially determined values.

longer than normal Fe–Cl bond does not compensate for the relatively small displacement of the Fe atom from the core; the average nonbonded Cl···N_{porph} distance of 3.186 (8) Å is significantly less than the previously supposed[19] minimum contact distance of 3.3 Å, being the sum of the van der Waals radii for chlorine and aromatic nitrogen. Contact distances less than the sum of the van der Waals radii are not unexpected between vicinally bonded atoms.

Thus, it is evident that the extension of both axial bonds, the position of the Fe atom, and the stereochemistry of the core are the results of a combination of subtle and interrelated crystallographically imposed factors, each of which influence and are influenced by the electronic state of the Fe.

Magnetic Properties of Solid Samples

A summary of the magnetic and ESR spectral properties of polycrystalline samples of the FeX(P-N_4) compounds is given in Table IV. Detailed discussion for each system is now given; in some cases more than one sample was investigated.

A. [FeCl(P-N_4)]·$CHCl_3$. Magnetic Susceptibilities. The magnetic susceptibilities of powdered samples were determined over the temperature range 4.2–300 K with a Faraday balance. Measurements were made on two preparations of the complex, and the results were very similar except for small differences in μ_{Fe} at 4.2 K, one sample showing 3.80 μ_B and the other 3.99 μ_B. A plot of μ_{Fe} vs. T is shown in Figure 4B, and tabulated data are given in Table V (supplementary material). Several features are noteworthy. The moment at 300 K is 5.68 μ_B, which is lower than the usual 5.9 μ_B expected for a mononuclear high-spin Fe(III) porphyrin of the Fe(porph)X type.[53,54] The temperature dependence of μ_{Fe}, though at first glance reminiscent of zero-field split d^5 behavior, does not conform in detail to that observed for hemin-like molecules such as Fe(TPP)Cl. In the latter case μ_{Fe} remains constant at ca. 5.9 μ_B until about 40 K, when it decreases, rapidly reaching ca.

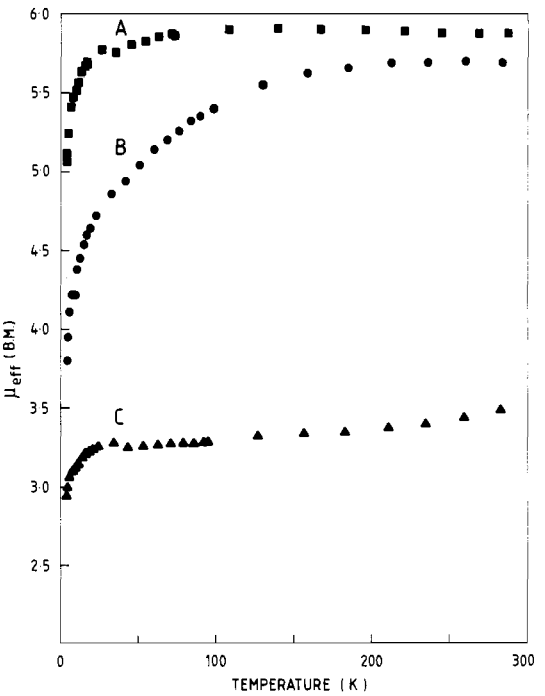

Figure 4. Experimental magnetic moments (μ_{eff} per Fe (μ_B)) for (A) [FeOH(P-N_4)]·$CHCl_3$, (B) [FeCl(P-N_4)]·$CHCl_3$ (sample 1), and (C) [FeN_3(P-N_4)]·MeOH.

4.8 μ_B at 4.2 K on account of a zero-field splitting parameter of magnitude $D \approx 6$ cm^{-1}.[54] In Figure 4B it can be seen that μ_{Fe} for the present compound starts to decrease below about 140 K, reaching 5.03 μ_B at 50 K and 3.9 μ_B at 4.2 K. The shape of the curve between 140 and 4.2 K is atypical of d^5 Fe(III) porphyrin behavior. Possible explanations for the observed temperature dependence of the magnetic susceptibility are given below.

Mössbauer Spectra. The Mössbauer spectrum of the first sample of FeCl(P-N_4)·$CHCl_3$ (Figure 5) shows a sharp asymmetric doublet at 300 K with isomer shift and quadrupole

(52) Tulinsky, A.; Chen, B. M. L. *J. Am. Chem. Soc.* **1977**, *99*, 3647.
(53) Maricondi, C.; Swift, W.; Straub, D. K. *J. Am. Chem. Soc.* **1969**, *91*, 5205.
(54) Behere, D. V.; Mitra, S. *Inorg. Chem.* **1979**, *18*, 1723.

Table III. Bond Angles (deg)[a]

atoms	angle	atoms	angle	atoms	angle	atoms	angle
						Fe-N(6)-C(29)	121.4 (6)
N(1)-Fe-N(3)	172.5 (3)	N(2)-Fe-N(4)	171.9 (3)	Cl-Fe-N(6)	177.7 (2)	Fe-N(6)-C(30)	121.9 (6)
N(1)-Fe-N(2)	89.2 (3)	N(2)-Fe-N(3)	89.6 (3)	N(3)-Fe-N(4)	90.2 (3)	N(4)-Fe-N(1)	89.9 (3)
N(1)-Fe-Cl	94.2 (2)	N(2)-Fe-Cl	95.6 (2)	N(3)-Fe-Cl	93.3 (2)	N(4)-Fe-Cl	92.5 (2)
N(1)-Fe-N(6)	86.8 (3)	N(2)-Fe-N(6)	86.5 (3)	N(3)-Fe-N(6)	85.7 (3)	N(4)-Fe-N(6)	85.4 (3)
Fe-N(1)-C(1)	125.6 (6)	Fe-N(2)-C(6)	125.1 (6)	Fe-N(3)-C(11)	126.3 (6)	Fe-N(4)-C(6)	125.9 (7)
Fe-N(1)-C(4)	126.3 (7)	Fe-N(2)-C(9)	127.0 (6)	Fe-N(3)-C(14)	125.4 (7)	Fe-N(4)-C(19)	127.0 (6)
C(1)-N(1)-C(4)	107.9 (8)	C(6)-N(2)-C(9)	107.4 (8)	C(11)-N(3)-C(14)	108.3 (8)	C(16)-N(4)-C(19)	106.3 (8)
N(1)-C(1)-C(2)	107.7 (9)	N(2)-C(6)-C(7)	107.5 (8)	N(3)-C(11)-C(12)	108.1 (9)	N(4)-C(16)-C(17)	107.6 (9)
N(1)-C(1)-C(20)	124.4 (10)	N(2)-C(6)-C(5)	127.1 (9)	N(3)-C(11)-C(10)	126.0 (9)	N(4)-C(16)-C(15)	124.4 (10)
C(2)-C(1)-C(20)	125.7 (11)	C(7)-C(6)-C(5)	125.4 (9)	C(12)-C(11)-C(10)	125.7 (10)	C(17)-C(16)-C(15)	127.9 (9)
C(1)-C(2)-C(3)	108.5 (10)	C(6)-C(7)-C(8)	107.2 (9)	C(11)-C(12)-C(13)	106.7 (10)	C(16)-C(17)-C(18)	109.2 (10)
C(2)-C(3)-C(4)	108.6 (9)	C(7)-C(8)-C(9)	108.3 (10)	C(12)-C(13)-C(14)	109.6 (9)	C(17)-C(18)-C(19)	107.0 (10)
C(3)-C(4)-N(1)	107.2 (9)	C(8)-C(9)-N(2)	109.6 (8)	C(13)-C(14)-N(3)	107.3 (9)	C(18)-C(19)-N(4)	109.8 (9)
C(3)-C(4)-C(5)	126.7 (9)	C(8)-C(9)-C(10)	126.1 (10)	C(13)-C(14)-C(15)	126.5 (9)	C(18)-C(19)-C(20)	124.1 (10)
N(1)-C(4)-C(5)	126.0 (9)	N(2)-C(9)-C(10)	124.3 (9)	N(3)-C(14)-C(15)	126.2 (9)	N(4)-C(19)-C(20)	126.0 (10)
C(4)-C(5)-C(6)	124.9 (9)	C(9)-C(10)-C(11)	126.4 (10)	C(14)-C(15)-C(16)	126.7 (9)	C(19)-C(20)-C(1)	124.6 (11)
C(4)-C(5)-C(21)	117.5 (8)	C(9)-C(10)-C(33)	116.5 (9)	C(14)-C(15)-C(45)	118.0 (9)	C(19)-C(20)-C(57)	119.9 (11)
C(6)-C(5)-C(21)	117.6 (9)	C(11)-C(10)-C(33)	117.0 (9)	C(16)-C(15)-C(45)	115.3 (9)	C(1)-C(20)-C(57)	115.3 (10)
C(5)-C(21)-C(22)	121.3 (8)	C(10)-C(33)-C(34)	123.0 (9)	C(15)-C(45)-C(46)	119.5 (9)	C(20)-C(57)-C(58)	115.8 (17)
C(5)-C(21)-C(26)	121.2 (9)	C(10)-C(33)-C(38)	117.6 (10)	C(15)-C(45)-C(50)	119.0 (9)	C(20)-C(57)-C(62)	123.6 (20)
C(22)-C(21)-C(26)	117.6 (9)	C(34)-C(33)-C(38)	119.4 (10)	C(46)-C(45)-C(50)	121.4 (10)	C(58)-C(57)-C(62)	120.4 (17)
C(21)-C(22)-C(23)	120.6 (8)	C(33)-C(34)-C(35)	121.6 (10)	C(45)-C(46)-C(47)	117.5 (10)	C(57)-C(58)-C(59)	128.7 (24)
C(21)-C(22)-N(5)	116.3 (8)	C(33)-C(34)-N(7)	116.1 (10)	C(45)-C(46)-N(9)	120.4 (9)	C(57)-C(58)-N(11)	117.6 (16)
C(23)-C(22)-N(5)	123.0 (8)	C(35)-C(34)-N(7)	122.2 (11)	C(47)-C(46)-N(9)	122.0 (10)	C(59)-C(58)-N(11)	113.5 (24)
C(22)-C(23)-C(24)	119.2 (9)	C(34)-C(35)-C(36)	118.3 (13)	C(46)-C(47)-C(48)	119.7 (11)	C(58)-C(59)-C(60)	96.3 (30)
C(23)-C(24)-C(25)	122.2 (10)	C(35)-C(36)-C(37)	122.9 (13)	C(47)-C(48)-C(49)	123.7 (11)	C(59)-C(60)-C(61)	141.3 (43)
C(24)-C(25)-C(26)	118.3 (10)	C(36)-C(37)-C(38)	119.9 (11)	C(48)-C(49)-C(50)	119.0 (11)	C(60)-C(61)-C(62)	110.9 (47)
C(25)-C(26)-C(21)	122.1 (10)	C(37)-C(38)-C(33)	117.8 (12)	C(49)-C(50)-C(45)	118.7 (10)	C(61)-C(62)-C(57)	119.1 (34)
C(22)-N(5)-C(27)	130.8 (8)	C(34)-N(7)-C(39)	130.4 (11)	C(46)-N(9)-C(51)	124.0 (10)	C(58)-N(11)-C(63)	137.6 (20)
N(5)-C(27)-O(1)	121.6 (9)	N(7)-C(39)-O(2)	123.5 (12)	N(9)-C(51)-O(3)	124.8 (13)	N(11)-C(63)-O(4)	117.6 (27)
N(5)-C(27)-C(28)	117.7 (9)	N(7)-C(39)-C(40)	116.0 (13)	N(9)-C(51)-C(52)	118.2 (12)	N(11)-C(63)-C(64)	116.1 (19)
O(1)-C(27)-C(28)	120.6 (9)	O(2)-C(39)-C(40)	120.3 (13)	O(3)-C(51)-C(52)	117.0 (14)	O(4)-C(63)-C(64)	124.7 (21)
C(27)-C(28)-C(29)	117.7 (8)	C(39)-C(40)-C(41)	122.2 (13)	C(51)-C(52)-C(53)	119.7 (12)	C(63)-C(64)-C(65)	127.2 (22)
C(27)-C(28)-C(32)	124.8 (9)	C(39)-C(40)-C(44)	119.7 (13)	C(51)-C(52)-C(56)	123.1 (12)	C(63)-C(64)-C(68)*	122.8
C(29)-C(28)-C(32)	117.4 (9)	C(41)-C(40)-C(44)	117.9 (13)	C(53)-C(52)-C(56)	116.9 (13)	C(65)-C(64)-C(68)*	108.7
C(28)-C(29)-N(6)	124.4 (9)	C(40)-C(41)-N(8)	122.0 (15)	C(52)-C(53)-N(10)	124.0 (13)	C(64)-C(65)-N(12)*	132.2
C(29)-N(6)-C(30)	116.7 (8)	C(41)-N(8)-C(42)	113.8 (14)	C(53)-N(10)-C(54)	115.9 (14)	C(65)-N(12)*-C(66)*	108.4
N(6)-C(30)-C(31)	123.5 (9)	N(8)-C(42)-C(43)	129.4 (15)	N(10)-C(54)-C(55)	125.6 (16)	N(12)*-C(66)*-C(67)*	124.6
C(30)-C(31)-C(32)	118.4 (10)	C(42)-C(43)-C(44)	115.2 (16)	C(54)-C(55)-C(56)	117.4 (15)	C(66)*-C(67)*-C(68)*	120.3
C(31)-C(32)-C(28)	119.6 (10)	C(43)-C(44)-C(40)	121.7 (14)	C(55)-C(56)-C(52)	120.0 (14)	C(67)*-C(68)*-C(64)	123.7
Cl(2)-C(69)*-Cl(3)	104.7	Cl(2)-C(69)*-Cl(4a)*	101.5	Cl(2)-C(69)*-Cl(4b)*	137.5	Cl(3)-C(69)*-Cl(4a)*	112.8
Cl(3)-C(69)*-Cl(4b)*	110.5	Cl(4a)*-C(69)-Cl(4b)*	42.8				

[a] Atoms marked with an asterisk were ill-defined and did not undergo sensible refinement. Their positional parameters were therefore held at their initially determined values.

Table IV. Summary of Magnetic Properties of [FeX(P-N_4)] Complexes in the Solid State

X	sample	magnetic moment, μ_B (μ_{Fe} (295 K))	magnetic moment, μ_B (μ_{Fe} (4.2 K))	spin state	ESR (4.2 K, powder)	features
Cl	1	5.69	3.80	$^5/_2$	rhombic high-spin signals with Fe-Fe coupled lines	linear-chain 6-coord structure; Cl-Fe---N axial ligation; rhombically distorted ligand field; nontypical high-spin magnetism; two $S = {}^5/_2$ Fe sites at 4.2 K from ESR, Mössbauer spectra; possible spin-crossover contribn
	2	5.61	3.99	$^5/_2$		
Br	1[a]	5.47	3.67	$^5/_2$	tetragonal high spin	similar to X = Cl; unusual asymmetry reversal in Mössbauer spectrum; less rhombic distortion in ESR than X = Cl
	2[b]	5.17	2.38	$^5/_2 \rightleftharpoons {}^1/_2$		magnetism typical of high-spin–low-spin crossover
OH		5.88	5.06	$^5/_2$	rhombic high spin	normal magnetic behavior; rhombically distorted ligand field; small hyperfine magnetic field in Mössbauer
N_3		3.49	2.94	$^5/_2 + {}^1/_2$	high-spin and low-spin signals	mixture of high-spin and low-spin forms present at all temp; magnetic moments much lower than for X = halide, hydroxide; kinetically controlled spin crossover probably operative with greater high-spin contribn above 160 K

[a] Crystallized with 10% hexane of solvation. [b] Crystallized from $CHCl_3$–toluene (see Experimental Section).

splitting values (Table VI) typical of $S = {}^5/_2$ Fe(III). The spectrum changes little at 77 K, but when the sample is cooled to 4.2 K, the line shape is compatible with the presence of two high-spin doublets, each with different δ and ΔE values with an area ratio of 70:30. The doublet with $\Delta E = 1.98$ mm s^{-1} is relaxing more rapidly than that with $\Delta E = 1.16$ mm s^{-1}. In an applied field of 25 kOe the 4.2 K spectrum splits as shown in Figure 5 and gives rise to a complex pattern con-

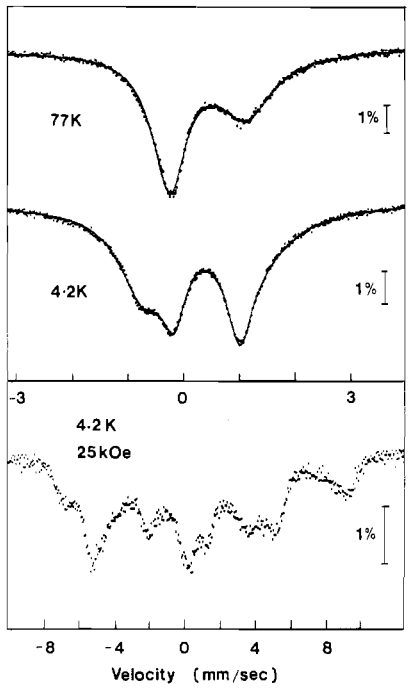

Figure 5. Mössbauer spectra of $[FeCl(P\text{-}N_4)]\cdot CHCl_3$ (sample 1) in zero applied field at 77 and 4.2 K and in 25 kOe applied field at 4.3 K. The solid lines are the fits using the parameters given in Table VI.

Table VI. Mössbauer Parameters for $FeX(P\text{-}N_4)$ Complexes

compd	T, K	δ, mm s^{-1} [a]	ΔE, mm s^{-1}	% area
$[FeCl(P\text{-}N_4)]\cdot CHCl_3$	77	0.43	1.35	100
(sample 1)	4.2	0.41	1.16	30
		0.24	1.89	70
$[FeCl(P\text{-}N_4)]\cdot CHCl_3$	4.2	0.44	1.27	*b*
(sample 2)		0.17	1.75	*b*
$[FeBr(P\text{-}N_4)]\cdot CHCl_3$	298	0.33	1.52	100
(sample 1)	77	0.45	1.59	100
	4.2	0.24	1.60	47
		0.39	2.31	53
$[FeOH(P\text{-}N_4)]\cdot CHCl_3$	298	0.3		*b*
	77	0.4		*b*
	4.2	0.42	0.16	100
$[FeN_3(P\text{-}N_4)]\cdot MeOH$	298	0.32	1.46	48
		0.20	2.07	52
	77	0.49	1.76	55
		0.30	2.30	45
	4.2	0.40	1.94	66
		0.28	2.32	33

[a] Relative to Fe at room temperature. [b] Difficult to estimate on account of overlapping lines.

sisting of more than six lines, indicating that more than one electronic state is involved. The maximum splitting yields an effective hyperfine field of 490 kOe, thus confirming the $S = {}^5/_2$ assignment. There is evidence for a second hyperfine field of ca. 320 kOe superimposed on the larger field.

The 4.2 K zero-field spectrum of the second sample showed parameters essentially similar to those of the first, the small differences in δ and ΔE being due to the uncertainty in fitting closely overlapping lines.

ESR Spectra. As indicated in our earlier communication,[6] this complex, as well as its related heterobinuclear Fe^{III}/Cu^{II} derivative, does not show an ESR spectrum at temperatures above ca. 50 K. This contrasts with the behavior of other hemin-like Fe(porphyrin)X molecules, which yield spectra at 77 K or above.[55] Line broadening and weakening of the

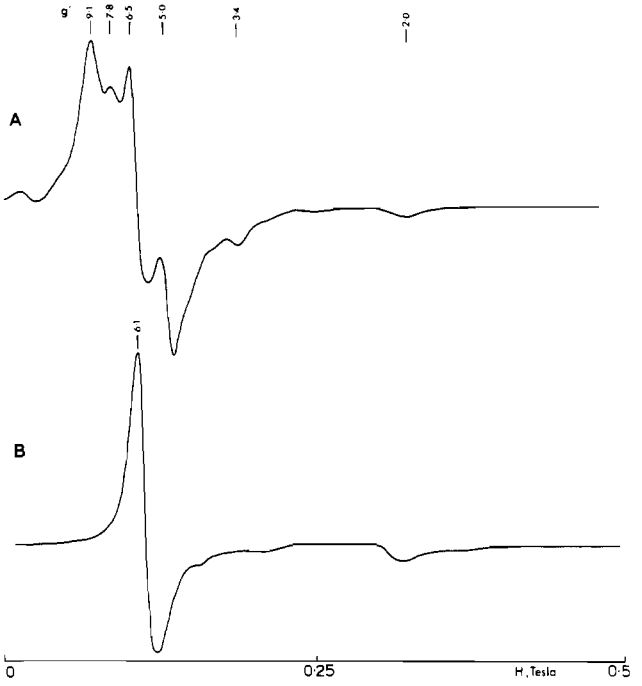

Figure 6. X-Band ESR spectra at 4.2 K of polycrystalline (powder) samples: (A) $FeCl(P\text{-}N_4)$; (B) $FeBr(P\text{-}N_4)$. The g' values describe the field–frequency relationship of the spectral lines and are not necessarily the true **g** tensors of the Zeeman term in the spin Hamiltonian.

present kind most probably arise through relaxation effects of the spin–spin type. At 40 K broad lines appear in the $g = 6$ and $g = 2$ regions as expected for tetragonally distorted high-spin Fe(III) porphyrins. The resolution is much improved at 4.2 K, where splitting of the $g_\perp = 6$ multiplet is now evident (Figure 6A), giving rise to peaks at $g = 9.1$, 7.8, 6.5, 5.0, and 3.4. There are two mechanisms that commonly give rise to splitting of a $g_\perp$ signal. The first is due to the presence of rhombic distortions[56] superimposed on the tetragonal ligand field, and this is likely to be operative in the solid-state spectrum of $[FeCl(P\text{-}N_4)]$ in view of its structure, although not necessarily so in fluid or frozen solution (vide infra). Rhombic splittings have been observed in a number of Fe(III) porphyrins such as mixed crystals of $Fe(TPP)Cl/TPPH_2$,[57] in various [Fe(porph)(SR)] complexes,[58] and in oxidized cytochrome P450,[59] although in none of these cases have the splittings been large enough to give lines as low in field as $g = 9.1$. Furthermore, if the present lines arise solely from rhombic splitting, then the number of lines indicates that two Fe(III) sites are possibly contributing to the spectrum at 5 K. The second reason for observing multiple lines is due to the presence of pairwise magnetic interactions between neighboring $S = {}^5/_2$ Fe(III) centers. Weak exchange coupling effects in high-spin Fe(III) porphyrins have recently been detected via ESR and susceptibility studies on polycrystalline and solution samples.[60,61] Lines at $g \approx 11.4$, 9.6, 3.6, and 3.0 were observed, for instance, in frozen toluene solutions of Fe(*m*-

(55) Palmer, G. In "The Porphyrins", Dolphin, D., Ed.; Academic Press: New York, 1979; Vol. IV, Chapter 6.
(56) Palmer, G. *Adv. Inorg. Biochem.* **1980**, *2*, 153.
(57) Sato, M.; Kon, H. *Chem. Phys.* **1976**, *12*, 199.
(58) Tang, C. S.; Koch, S.; Papaefthymiou, G. C.; Foner, S.; Frankel, R. B.; Ibers, J. A.; Holm, R. H. *J. Am. Chem. Soc.* **1976**, *98*, 2414.
(59) Tsai, R.; Yu, C. A.; Gunsalus, I. C.; Peisach, J.; Blumberg, W.; Orme-Johnson, W. H.; Beinert, H. *Proc. Natl. Acad. Sci. U.S.A.* **1970**, *66*, 1157.
(60) Chikira, M.; Kon, H.; Smith, K. M. *J. Chem. Soc., Dalton Trans.* **1980**, 526.
(61) Ernst, J.; Subramanian, J.; Fuhrhop, J. H. *Z. Naturforsch., A* **1977**, *32A*, 1129.

$NO_2OEP)Cl$,[60] while lines at $g \approx 10.4$, 5.8, 3.6, and 3.2 were reported for powdered samples of Fe(OEP)Cl at 4.2 K.[61] In the present compound we feel that the ESR line shape at 4.2 K is due to contributions from both rhombic distortions and from weak Fe^{III}–Fe^{III} coupling effects. Further discussion is given below in conjunction with the magnetic results.

Data Analysis and Discussion. Despite the small differences in magnetism and Mössbauer parameters described above, we feel that the two samples of $FeCl(P\text{-}N_4)\cdot CHCl_3$ have essentially the same electronic structure and can be described by the same magnetic model. A number of approaches were instigated before arriving at a satisfactory model that could encompass the structural, susceptibility, and Mössbauer and ESR spectral results.

In trying first to rationalize the magnetic data, it is possible to envisage a number of reasons that could explain μ_{Fe} values that are less than 5.92 μ_B at room temperature and that display the atypical temperature dependence described. They are (i) a large rhombic component in the ligand field, i.e., $E/D > 0$ (see below), (ii) the presence of a spin crossover involving $S = {}^3/_2$ or $S = {}^1/_2$ Fe(III) states, (iii) the presence of some impurity that would lower μ_{Fe}, e.g. a strongly coupled μ-oxo dimer, and (iv) weak antiferromagnetic exchange interactions between neighboring Fe centers within the chainlike structure.

Reason i can be eliminated, at least in terms of a single monomeric species, since it was not possible to fit the magnetic data to either an axial or rhombic spin Hamiltonian. We have shown recently that, while a rhombic ligand field component can influence the shape of μ/T at low temperatures, it has minimal effects on the size of μ_{Fe} at ambient temperatures.[62] The present compound does possess rhombic symmetry, and this is described further under reason iv. The second hypothesis is that the reduction in the moments at high temperatures could be due to a "spin equilibrium" of some kind. A dynamic thermal equilibrium between $S = {}^5/_2$ and $S = {}^1/_2$ (or $S = {}^3/_2$) states, commonly observed in solutions of Fe(III) spin-crossover complexes, can be eliminated since the χ/T data do not yield a linear log K vs. $1/T$ plot, where K is the equilibrium constant. It seems likely that spin-crossover behavior of the type observed in solid samples of Fe(III) tris(dithiocarbamates) and Fe(III) Schiff-base species,[25] as well as in sample 2 of $FeBr(P\text{-}N_4)$ described below, is not occurring. However, it is difficult to exclude this possibility entirely. As pointed out recently by Hendrickson et al.,[25] solid samples of Fe(III) spin-crossover compounds that display non-Boltzmann magnetic behavior do not generally experience an equilibrium situation, because of kinetic control. These authors favor a nucleation and growth mechanism in which molecules of one spin state grow within those of the other spin state at the crossover transition. Various subtle effects in the solid state such as crystallite size, crystal defects, pressure, presence of solvate molecules, etc. can influence the spin transition and hence the magnetism. While the ESR and Mössbauer spectra in Figures 5 and 6 would militate against a spin crossover in the present sample, it is possible that nonequilibrium behavior of the type described and/or unfavorable relaxation rates prevent observation of lines from both high- and low-spin states. Alternative "quantum mechanically mixed spin" models have been developed by a number of authors to incorporate the interactions of the high-spin ground state with low- and/or intermediate-spin excited states via spin–orbit coupling, interelectronic repulsion, and ligand field effects.[24,26,63–66] These models vary in their

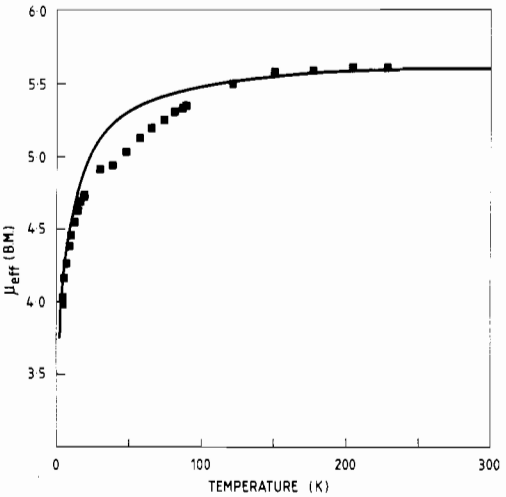

Figure 7. Comparison of experimental magnetic moments for $[FeCl(P\text{-}N_4)]\cdot CHCl_3$ (sample 2) with calculated values (solid line) using the Maltempo model[24] ($^6A_1$–$^4A_2$ separation 500 cm^{-1}; spin–orbit coupling constant $\zeta = 300$ cm^{-1}).

level of theoretical sophistication, but all relate to a single magnetic species being present. We have employed the model of Maltempo,[24] which is limited to $S = {}^5/_2$ and $S = {}^3/_2$ states, for the present chloro complex and obtain the fit shown in Figure 7. The calculated curve is appropriate to an energy separation of 500 cm^{-1} between the high-spin and intermediate-spin states. While the fit is generally not too bad, it fails to agree with the slope of the curve in the region 30–80 K. The observed ESR "g" values also do not agree with those calculated from the Maltempo model, viz. 5.6 and 2.0. Further, since the 4.2 K Mössbauer spectrum is compatible with the presence of two distinct $S = {}^5/_2$ sites, it is possible to eliminate the mixed-spin description.

Although it is always difficult to be absolutely sure that chemical impurities have not cocrystallized in Fe(III) porphyrins of the present kind (reason iii), we feel that this is not the reason for the present results. The most obvious contaminant would be the ubiquitous μ-oxo dimer, whose low magnetic moment (generally ca. 1.9 μ_B/Fe)[67] and high-spin Mössbauer lines could perhaps explain the magnetic and Mössbauer data. However, the absence both of ν(FeOFe) bands in the IR spectrum and of characteristic visible electronic bands (Table 10), as well as the nature of the preparation and purification procedures used, militate strongly against this proposal. The presence of any contaminating $FeOH(P\text{-}N_4)$ species can also be eliminated in view of its magnetic, Mössbauer, and spectral properties (vide infra).

Bearing in mind the reservations discussed above with respect to a possible spin-crossover contribution, we are left with reason iv, the presence of weakly coupled interactions, as the remaining and preferred description, although we need to assume the coexistence of monomeric and polymeric $[FeCl(P\text{-}N_4)]$ moieties in the crystalline samples to obtain a complete picture. Preliminary calculations using a simple Heisenberg dimer Hamiltonian $-2J\hat{S}_1\cdot\hat{S}_2$ (where $S_1 = S_2 = {}^5/_2$) predict a magnetic moment of 5.6 μ_B at 300 K for $J \approx -3$ cm^{-1}, which decreases to 1.1 μ_B at 4.3 K, quite at variance with the observed value of 3.9 μ_B at 4.3 K. Inclusion of zero-field splitting terms does not improve the situation at low temperatures. Calculations were then made using a Heisenberg chain model, which is more appropriate to the crystal structure described above. In preliminary stages the susceptibilities were calculated by means of eq 1, which was conveniently rearranged to the ratio

(62) Berry, K. J.; Clark, P. E.; Murray, K. S.; Raston, C. L.; White, A. H. *Inorg. Chem.*, in press.
(63) Harris, G. *Theor. Chim. Acta* **1968**, *10*, 119, 155.
(64) Boyd, P. D. W.; Buckingham, D. A.; McMeeking, R. F.; Mitra, S. *Inorg. Chem.* **1979**, *18*, 3585.
(65) Caro, P.; Faucher, M.; Savy, M.; Pankowska, H. *J. Chem. Phys.* **1978**, *68*, 1045.
(66) McMeeking, R., unpublished calculations, 1980.
(67) Murray, K. S. *Coord. Chem. Rev.* **1974**, *12*, 1.

$$\chi = f\chi_{HS} \quad (1)$$

$$f' = \chi/\chi_{HS} \quad (2)$$

$$\mathcal{H} = D[\hat{S}_z^2 - S(S+1)/3] + E(\hat{S}_x^2 - \hat{S}_y^2) + g\beta\hat{H}\cdot\hat{S} \quad (3)$$

$$f = (1+U)/(1-U) \quad (4)$$

$$U = \coth(2JS(S+1)/kT) - kT/2JS(S+1)$$

given in eq 2 in order to test out the model. In these equations χ_{HS} was calculated for $S = {}^5/_2$ iron(III) following computer diagonalization of the matrix obtained from the operation of the spin Hamiltonian (3) on the $^6A_1$ basis function set.[62] The function, f, given in (4) is that defined by Fisher for a Heisenberg chain.[68]

It was found experimentally that the ratio f' did not vary as significantly with temperature as this model would require if it were the dominant perturbation on the system. In an attempt to overcome this poor agreement, calculations were then made with the assumption that *two* species of [FeCl(P-N_4)] were present, one a high-spin monomer, the other a high-spin Heisenberg chain of the type just described. This was achieved with use of eq 5, in which α is the fraction of monomer present.

$$\chi = \chi_{HS}[\alpha + (1-\alpha)f] \quad (5)$$

In order to reduce the number of variable parameters, the zero-field parameters D and E were assumed to be the same in both the monomeric and coupled species, which seems reasonable. A good fit of the μ_{Fe}/T data was accomplished as shown in Figure 8. The best-fit parameters were

$$D = 10 \pm 0.5 \text{ cm}^{-1} \qquad E = 2.25 \pm 0.25 \text{ cm}^{-1}$$
$$J = -5 \pm 0.2 \text{ cm}^{-1} \qquad \alpha = 0.70 \pm 0.02$$

This model achieves reasonable consistency between the magnetic, Mössbauer, and ESR results. Thus, the value of α is close to the relative areas observed for the two high-spin doublets in the Mössbauer spectrum. The small differences in δ and ΔE values for these two doublets can be ascribed to the presence of monomeric chain sites in which the iron porphyrin molecules have similar, but not identical, electronic and geometric environments. In the case of the ESR spectrum, the g values calculated by using, for instance, $D = 10$ cm^{-1} and $E = 2.5$ cm^{-1} (i.e., $E/D = 0.25$) are $g_z = 4.8$, $g_x = 4.1$, $g_y = 3.8$, and $g_y' = 9.4$, which are in quite good agreement with the observed lines. The line observed at $g = 7.8$ is probably due to exchange-coupled Fe(III) centers within the chain species. It is possible that the $g = 3.4$ line might also arise from Fe–Fe interaction since lines in this position have been observed previously in various high-spin Fe(III) porphyrins.[60] In one such study on frozen aqueous alkaline–Me_2SO solutions of hemin there was considerable similarity in the $g \approx 6$ region to that shown in Figure 6A. The authors gave a tentative assignment similar in many respects to that proposed here.[60]

In summarizing the electronic features of [FeCl(P-N_4)] in the solid state, we have seen that it behaves in a rather atypical and unusual manner when compared to its behavior in solution and when compared to many other hemin-like Fe(III) porphyrin systems. The occurrence of monomeric and associated species in the polycrystalline samples may be related to the presence of chloroform of solvation in the lattice or to the disposition of the Cl^- ligand either inside or outside the "pocket" formed by the four pyridine ligands; a polymeric structure is sterically prohibited in a species in which the Cl^- occupies an "outside" position. While the crystal chosen for X-ray diffraction study displayed only the polymeric chain molecular structure at 295 K, it is possible that bulk samples contain both species. The possibility of other atropisomers in the sample is discounted, as discussed in the Experimental Section and Synthesis and Reactions. A recent study of [Fe(TPP)(SPh)·PhSH] likewise showed a somewhat related and even more complicated mixture of magnetic species in the solid phase.[5] Exchange interactions have, as noted earlier, been detected in a number of chloro iron(III) porphyrins.[60,61] Temperatures lower than 4.2 K have usually been required in order to detect such interactions by susceptibility methods since the J values were less than 1 cm^{-1}. It is interesting to note that Fe(TPP)Cl has been regarded as being made up of 50% monomeric and 50% dimeric molecules; i.e., $\alpha = 0.5$.[69] The magnitude of the coupling in the present complex is somewhat high when compared to those of other Fe(III) porphyrins and when considered in terms of the extended exchange pathway shown in Figure 2. Unfortunately, there are no other examples of bridging groups of this kind for comparison. A possible alternative explanation is that the structurally characterized polymeric component has $J = 0$, while the coupled component incorporates chloro bridging of some kind; this may also account for the apparent J dependence on the axial group X in FeX(P-N_4), where X = Cl, Br (see below).

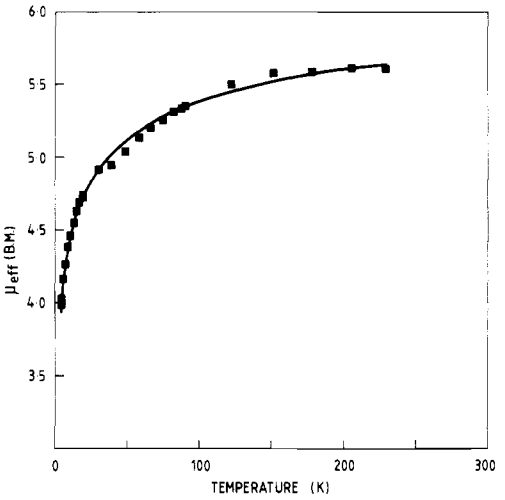

Figure 8. Best fit calculated curve for [FeCl(P-N_4)]·$CHCl_3$ (sample 2) using model described in text, which incorporates a fraction, $\alpha = 0.7$, of $S = {}^5/_2$ monomeric molecules with the remainder being $S = {}^5/_2$ Heisenberg linear-chain molecules. The spin Hamiltonian parameters in both components are $D = 10$ cm^{-1}, $E = 2.5$ cm^{-1}. The exchange coupling constant in the chain, J, is -5 cm^{-1}.

B. [FeBr(P-N_4)]·$CHCl_3$. Magnetic Susceptibility and ESR Spectra. Considerable difficulty was experienced in obtaining the bromo complex free from about 10% of hexane of solvation, the solvent initially used to precipitate the crystals. Susceptibility data were collected on two samples, the first of which contained hexane of solvation while the second, which was crystallized from chloroform/toluene, did not (see Table VII, supplementary material). There are dramatic differences in the μ/T data between the two samples (Figures 9 and 10), and in neither case is the behavior typical of a high-spin iron(III) porphyrin such as Fe(TPP)Br. In fact the reciprocal susceptibility and magnetic moment plots of sample 2 are indicative of spin-crossover behavior involving high-spin and low-spin states. The "minimax" dependence of μ_{Fe} and the corresponding temperature dependence of the moment shown

(68) Fisher, M. E. *Am. J. Phys.* **1964**, *32*, 343.

(69) Neiheisel, G. L.; Imes, J. L.; Pratt, W. P., Jr. *Phys. Rev. Lett.* **1975**, *35*, 101.

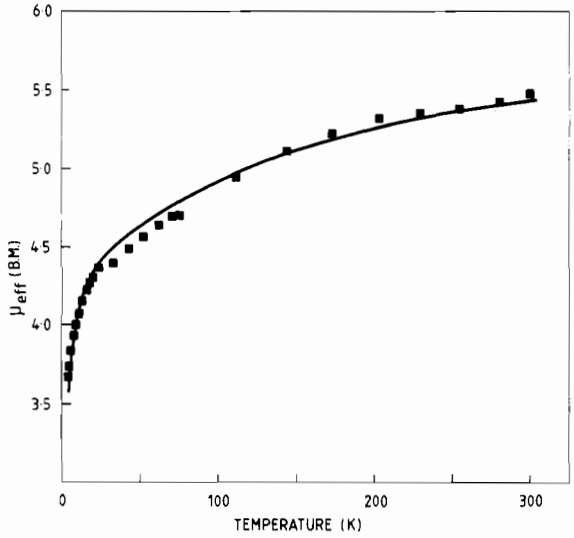

Figure 9. Experimental and calculated magnetic moments for [FeBr(P-N_4)]·$CHCl_3$ (sample 1, which contains 10% hexane of solvation). The solid line is the calculated best fit using the parameters $\alpha = 0.57$, $D = 10$ cm^{-1}, $E = 0.8$ cm^{-1} and J(within the chain) $= -8$ cm^{-1}.

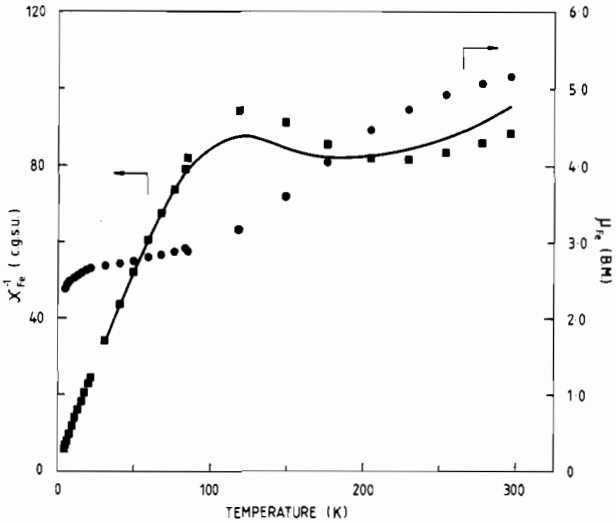

Figure 10. Experimental and calculated magnetic moments for [FeBr(P-N_4)]·$CHCl_3$ (sample 2). The solid line is the calculated best fit to a spin-equilibrium model[70] using the parameters $g(^2T_{2g}) = 2.21$, $\lambda(^2T_{2g}) = 340$ cm^{-1}, $\Delta E(^6A_{1g}-^2T_{2g}) = 80$ cm^{-1}, and $C = 4.0$.

in Figure 10 (5.17 μ_B at 296 K, 2.38 μ_B at 4.3 K) parallel closely the spin-crossover behavior observed in the octaethylporphyrin bisadduct [Fe(OEP)(3-Cl-py)$_2$](ClO_4)[26,70] and in various tris(dithiocarbamato)iron(III) chelates.[71] The magnetic behavior of sample 1 is generally similar to that of [FeCl(P-N_4)]·$CHCl_3$ described above. The differences in the susceptibilities of the two samples are most likely related to the presence of chloroform and hexane molecules in the crystal lattice. There are now well-documented examples of iron porphyrins and iron dithiocarbamates whose magnetic properties are very sensitively perturbed by the presence of solvate molecules. It is also possible that slightly different crystal phases result from the different crystallizing media.

The ESR spectrum of a powdered sample of [FeBr(P-N_4)] at 10 K shows a line shape typical of that expected for high-spin Fe porphyrins with a weak line at $g = 2$ and a strong line at $g = 6.1$. The latter line does not show the degree of rhombic splitting exhibited by the chloro derivative (Figure 6B).

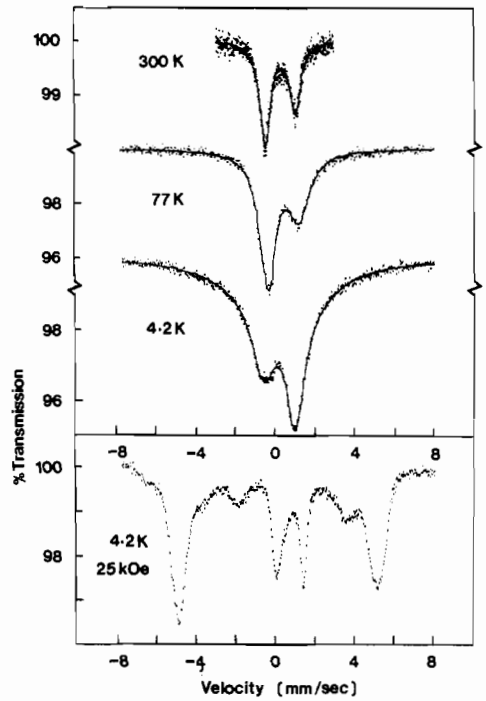

Figure 11. Mössbauer spectra of [FeBr(P-N_4)]·$CHCl_3$ (sample 1) in zero applied field at 300, 77, and 4.2 K, and in 25 kOe applied field at 4.2 K. The solid lines are the fits using the parameters given in Table VI.

Mössbauer Spectra. The zero-field Mössbauer spectra of the first sample of [FeBr(P-N_4)]·$CHCl_3$ show some interesting effects (Figure 11). At room temperature the spectrum consists of an asymmetric doublet in which the asymmetry is thought to originate chiefly from relaxation broadening with perhaps a small contribution from texture effects. The isomer shift and quadrupole splitting, $\delta = 0.33$ mm s^{-1} and $\Delta E = 1.52$ mm s^{-1}, are of magnitudes similar to those of [FeCl(P-N_4)]. The δ value is in the normal range for $S = {}^5/_2$ iron(III) porphyrins while the ΔE value is much larger and no doubt reflects the particular ligand field of the (P-N_4) series. Between room temperature and 77 K the lines broaden a little and the δ and ΔE values increase slightly. Then at 4.2 K there is a reversal in the intensities of the lines, which can be clearly seen in Figure 11. At the same time, the lines broaden as a result of the decrease in relaxation rate. This reversal in asymmetry has been observed in other high-spin iron(III) porphyrins of the type Fe(porph)X (where porph = tetraphenylporphyrin and tetrakis(*p*-methoxyphenyl)porphyrin) and has been discussed in detail by Sams and Tsin.[72] In essence it is a result of temperature-dependent broadening mechanisms, which affect the low- or high-velocity lines differently at different temperatures. In principle it is possible to estimate the zero-field splitting, D, from the spectrum in which the lines are symmetrical, but we unfortunately do not have this spectrum available. In order to get the good fit shown in Figure 11 for the 4.2 K spectrum, a second quadrupole doublet was included, which had a larger ΔE value than that of the main doublet. However, the existence of a second low-temperature site in the bromo complex is not as obvious as it is in the chloro derivatives (Figure 5). In the latter a second doublet is clearly displayed while in the former broad wings occur on the main doublet.

The Mössbauer spectrum at 4.2 K of this bromo sample in a longitudinal field of 25 kOe is also shown in Figure 11. The magnetic hyperfine splitting, though somewhat asymmetric

(70) Fitzroy, M.; Murray, K. S., unpublished data.
(71) Martin, R. L.; White, A. H. *Transition Met. Chem. (N.Y.)* **1968**, *4*, 113.
(72) Sams, J. R.; Tsin, T. B. In "The Porphyrins"; Dolphin, D., Ed.; Academic Press: New York, 1979; Vol. IV, p 425 ff.

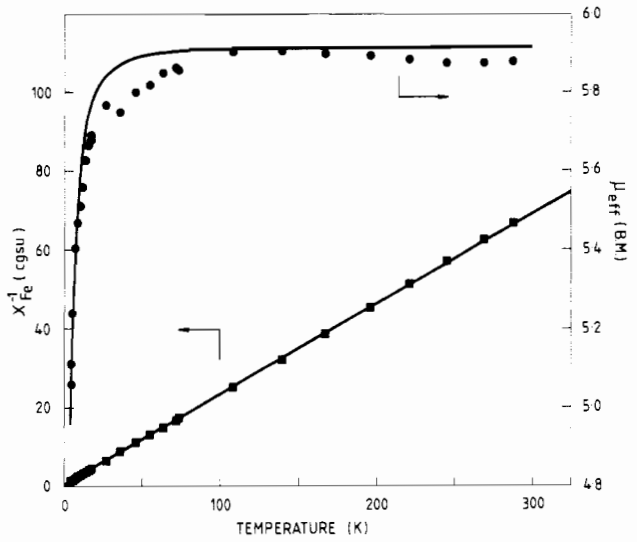

Figure 12. Experimental magnetic moments, and reciprocal susceptibilities, for [FeOH(P-N_4)]. The solid line is the calculated best fit using the spin Hamiltonian parameters D = 5.3 cm^{-1}, E = 0.05 cm^{-1}.

in overall shape, is quite well resolved and similar to that displayed by other high-spin Fe(III) porphyrins that possess a $M_s = \pm^1/_2$ Kramers ground level.[73] The effective field at the nucleus H_{eff} is 310 kOe, which is smaller than that in [FeCl(P-N_4)]·$CHCl_3$ but of magnitude similar to those observed in some tetrakis(*p*-methoxyphenyl)porphyrin complexes.[72] Comparison of the applied-field spectra of the bromo and chloro compounds shows that if two Fe(III) sites coexist at 4.2 K in the bromo derivative then they are very similar in their electronic and geometric arrangements.

Unfortunately we do not have Mössbauer measurements on the second sample of [FeBr(P-N_4)]·$CHCl_3$.

Data Analysis. The magnetic data for the first sample of [FeBr(P-N_4)] were analyzed with use of the model developed for the chloro complex, and a good fit to the data was obtained (Figure 9). Approximately 57% of the molecules were assumed to be present as high-spin monomers with the remainder present as polymeric linear chains. The zero-field splitting parameters and antiferromagnetic coupling constant were found to be

$$D = 10\ cm^{-1} \qquad E = 0.8\ cm^{-1} \qquad J = -8\ cm^{-1}$$

The lower E value means that the symmetry of the ligand field around Fe in this compound is closer to tetragonal than it is in the chloro complex, which is in line with the ESR spectral line shape. A larger value of J is required to explain the more pronounced temperature dependence of μ_{Fe} for [FeBr(P-N_4)] compared to that for [FeCl(P-N_4)]. It is not obvious why the chain component in the bromo complex should be more strongly coupled than the chloro complex unless the halide group in some way participates in a superexchange pathway, as discussed above.

The second sample of [FeBr(P-N_4)] displays a temperature dependence of μ_{Fe}, which is symptomatic of spin-crossover behavior. Compared to other such values in Fe(III) porphyrins[26] and tris(dithiocarbamate) complexes,[71] the moment at room temperature, 5.17 μ_B, is higher than usual while the low-temperature plateau value, ca. 2.7 μ_B, is also a little high. These effects might be due to the presence of a small amount of high-spin species of the type found in the first sample or to an incomplete spin transition.[25] We have analyzed the μ_{Fe} data by means of the simple noninteracting model developed by Martin and Golding and co-workers[71,74] and later extended by Hendrickson.[75] Since the appropriate energy levels of the high-spin $^6A_1$ and low-spin $^2T_2$ states and the equation for μ_{Fe} have been given elsewhere,[71] they will not be reproduced here. Suffice it to say that a number of assumptions are implicit in this model, not the least of which are the assumptions of octahedral symmetry and noninteraction (via spin–orbit coupling) of the energy levels. With these reservations in mind we see from Figure 10 that a reasonable fit to the data was obtained. The best-fit parameters were as follows: g(low-spin state) = 2.21; λ(spin–orbit coupling constant of $^2T_2$ state) = −340 cm^{-1}; ΔE(zero-point energy difference $^6A_1 - {}^2T_2$) = 80 cm^{-1}; C(ratio of vibrational partition functions of the high- and low-spin molecules) = 4.0. These values are comparable to those similarly deduced for the six-coordinate hemichrome [Fe(OEP)(3-Cl-py)$_2$](ClO_4).[70] The energy levels appropriate to these parameters are

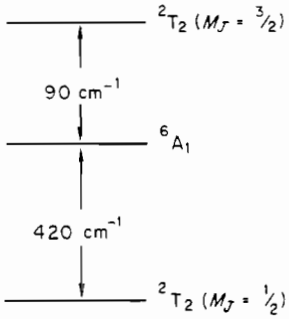

Low-symmetry splitting of both $^6A_1$ and $^2T_2$ states will, of course, further perturb these levels. While a more complete treatment of the data using the interacting "mixed-spin" model developed by Harris,[63] Gregson,[26] and McMeeking[66] might be desirable, the essential message is clear. It is that the energies of the high- and low-spin states are very close together. This leads to both states being thermally populated at high temperatures but only the low-spin levels at low temperatures. The chemical or structural reasons for spin-crossover behavior in the second sample cannot be ascertained with certainty without a crystal structure determination, but one would predict the iron porphyrin geometry to be related to that observed in the magnetically similar complex [Fe(OEP)(3-Cl-py)$_2$](ClO_4).[23] The chloroform solvate molecule presumably plays a subtle but significant role.

C. [FeOH(P-N_4)]·$CHCl_3$. Magnetic susceptibilities of two independently prepared samples of this hematin analogue were investigated, the variations of μ_{Fe} with temperature being similar in each case and clearly symptomatic of a zero-field-split $^6A_1$ ground state (Table VIII (supplementary material) and Figure 4A). There was evidence for a slight mass loss occurring in the Faraday bucket at temperatures greater than 250 K, most likely due to loss of some solvated chloroform. The moment remains essentially constant at ca. 5.9 μ_B between 300 and 40 K before decreasing to 5.06 μ_B at 4.2 K. The corresponding μ_{Fe}/T plot is linear and Curie-like, i.e. $\Theta = -1.3$ K. The 4.2 K ESR spectrum of a powdered sample is shown in Figure 13A. A broad low-field line peak at g = 6.4 is centered at g = 4.5 and shows a rather unusual line shape, which can probably be accounted for by a combination of rhombic splitting and aggregation in the solid state. The $g_\parallel$ line at 2.0 can just be discerned. The spectrum broadens and weakens as the temperature is raised to 30 K such that above

(73) Fitzsimmons, B. W.; Sams, J. R.; Tsin, T. B. *Chem. Phys. Lett.* **1976**, *38*, 588. Dolphin, D. H.; Sams, J. R.; Tsin, T. B.; Wong, K. L. *J. Am. Chem. Soc.* **1978**, *100*, 1711.

(74) (a) Ewald, A. H.; Martin, R. L.; Ross, I. G.; White, A. H. *Proc. R. Soc. London, Ser. A* **1964**, *280*, 235. (b) de Lisle, J. M.; Golding, R. M. *Ibid.* **1967**, *296*, 457.

(75) Hall, G. R.; Hendrickson, D. N. *Inorg. Chem.* **1976**, *15*, 607.

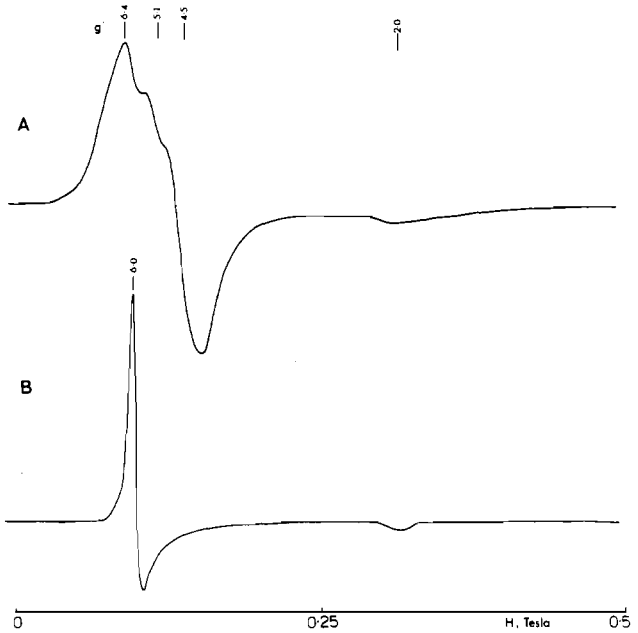

Figure 13. X-Band ESR spectra at 4.2 K of FeOH(P-N_4): (A) polycrystalline (powder) sample; (B) Me_2SO frozen solution.

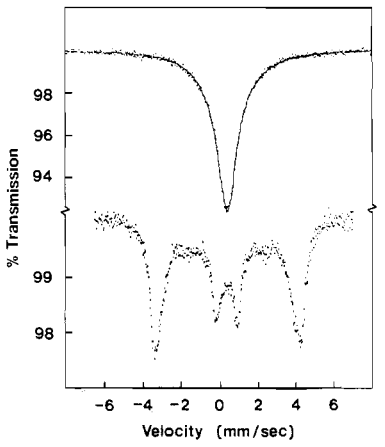

Figure 14. Mössbauer spectra of [FeOH(P-N_4)]·$CHCl_3$ at 4.2 K in zero applied field and in 25 kOe applied field.

ca 40 K the lines again disappear. The observed magnetic moments were compared to those calculated by using the spin Hamiltonian given in eq 3. The best fit curve is shown in Figure 12, and the corresponding zero-field splitting parameters are

$$D = 5.3 \pm 0.1 \text{ cm}^{-1} \qquad E = 0.05 \pm 0.05 \text{ cm}^{-1}$$

The total zero-field splitting and the rhombicity are lower than those deduced for the chloro and bromo derivatives.

The zero-field Mössbauer spectrum at 4.2 K is shown in Figure 14. The spectrum consists of a quadrupole doublet with an extremely small ΔE value of 0.16 mm s^{-1}, the constituent lines having equal area but different line widths. The magnitude of the isomer shift, $\delta = 0.42$ mm s^{-1}, confirms the spin state to be $^5/_2$. As the temperature is raised, the higher energy line broadens preferentially, indicating that $V_{zz} > 0$. The rate of relaxation decreases with increasing temperature until it is comparable with the Larmor precessional frequency, and a single broad non-Lorentzian line results at high temperature (not shown). This behavior is compatible with a positive zero-field splitting, $D > 0$, in which the $M_s = \pm^1/_2$ state is occupied at 4.2 K and has a fast relaxation time. At higher temperatures the $\pm^3/_2$ and $\pm^5/_2$ states become populated, and since these have longer relaxation times, the spectrum becomes asymmetric. This kind of behavior has been observed in various hemin molecules, although the present compound appears to show the asymmetry at a temperature lower than has been reported previously.[72,73] The spectrum in an applied field of 25 kOe at 4.2 K is also shown in Figure 14. Only four of the hyperfine lines are resolved while the spread of the lines corresponds to a small H_{eff} of ca. 236 kOe, which is less than those for [FeX(P-N_4)] (X = Cl, Br) but comparable with that for Fe(*p*-MeOTPP)I.[72] Clearly there are a number of factors that combine to produce these variations in H_{eff}. In the present P-N_4 series the order of decreasing H_{eff} is Cl > Br > OH, which is similar to the order of decreasing ΔE, viz. Cl ≈ Br > OH. A dependence of the magnetic hyperfine constant on the nature of the axial ligand in some high-spin Fe(III) porphyrins has also been found by Holm, Frankel, et al.[58] and by Sams et al.[72,73] Interestingly, in three Fe(PPIXDME)(XR) complexes the alkoxide (XR = OCH_3) gave a larger hyperfine constant than the arenethiolate (XR = $SC_6H_4NO_2$) with a general expectation of the saturation hyperfine field for anionic oxygen ligation being >500 kOe.[58] In contrast, the OH^- axial ligand here shows a saturation field of only 313 kOe (assuming $g_\perp = 6$), which seems to contradict this trend even with allowance for the difference of in-plane porphyrin ligand. Unfortunately there are presently no other hydroxy derivatives available for comparison.

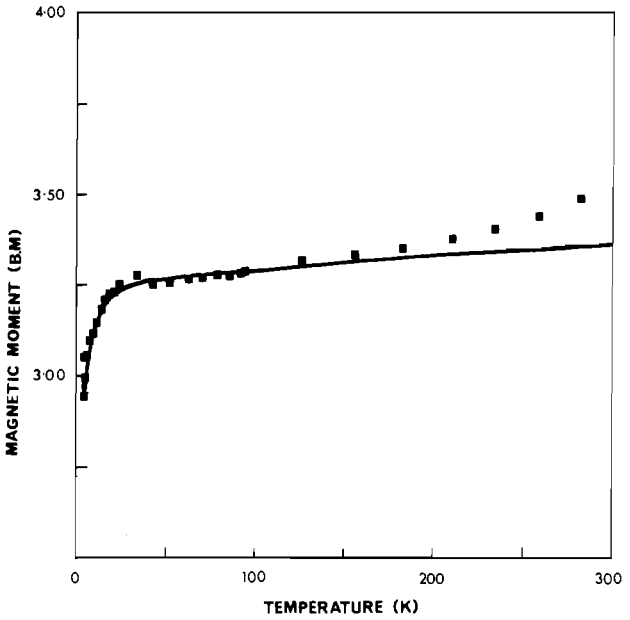

Figure 15. Experimental (■) and calculated (solid line) magnetic moments for [FeN_3(P-N_4)]·CH_3OH. The solid line includes a low-lying state at 550 cm^{-1} for both the high-spin and the low-spin molecules.

D. [FeN_3(P-N_4)]·CH_3OH. μ_{Fe} values for the azido complex are markedly different from those of the Cl, Br, and OH derivatives. (Table IX, supplementary material). As seen in Figure 4C, μ_{Fe} decreases only a little from 3.49 μ_B at 283 K to 3.23 μ_B at 18 K, then more rapidly reaching 2.94 μ_B at 4.3 K. A plot of $1/\chi_{Fe}$ vs. T shows Curie–Weiss behavior between 4.2 and 95 K with Θ of −1 K, while above this range there is gentle curvature. In the absence of any other data one suspects the possible existence of either intermediate-spin Fe(III) ($S = ^3/_2$), a spin crossover involving spin states other than $^5/_2$, or a mixture of high-spin and low-spin molecules. The ESR spectrum of the powder at 4.2 K (Figure 16) shows lines due to high-spin and low-spin Fe(III) species, which immediately eliminates the intermediate-spin possibility.

Zero-field Mössbauer spectra, shown in Figure 17, indicate the presence of two quadrupole doublets at all temperatures. δ and ΔE values are given in Table VI. At 298 K the two

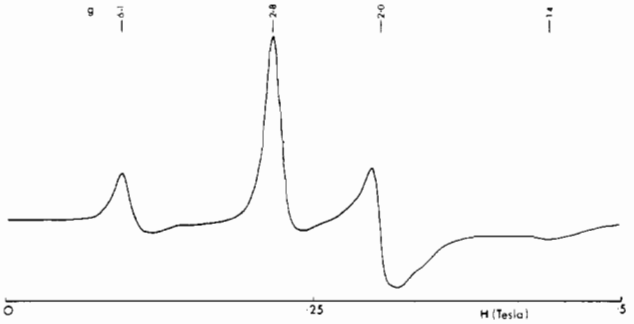

Figure 16. X-Band ESR spectrum at 4.2 K of polycrystalline (powder) $[FeN_3(P\text{-}N_4)]\cdot MeOH$.

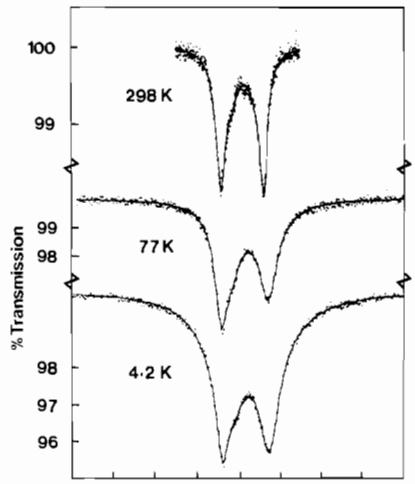

Figure 17. Mössbauer spectra for $[FeN_3(P\text{-}N_4)]\cdot MeOH$ in zero applied field at 298, 77, and 4.2 K. The solid lines are the fits using the parameters given in Table VI.

doublets have parameters $\delta_1 = 0.20$ mm s^{-1}, $\Delta E_1 = 2.07$ mm s^{-1}, $\delta_2 = 0.32$ mm s^{-1}, $\Delta E_2 = 1.46$ mm s^{-1} and are of equal area. When the sample is cooled to 4.2 K, the area ratio of doublet 1/doublet 2 decreases to 1/2. There are concomitant small shifts in δ and ΔE values, with the quadrupole splitting of doublet 2 increasing in particular from 1.46 to 1.94 mm s^{-1}. By analogy with the other complexes already discussed, doublet 2 is assigned to high-spin Fe(III) while doublet 1 is typical of low-spin Fe(III) porphyrins.

All the data therefore point to the coexistence of $S = {}^5/_2$ and $S = {}^1/_2$ Fe(III) sites resulting from spin-crossover behavior. The Mössbauer and ESR spectra show that the ratio of high- to low-spin molecules does not change markedly as a function of temperature, which strongly suggests that kinetic control is present, as discussed above in relation to $FeCl(P\text{-}N_4)$. In other words, the rate of spin-state interconversion is such that equilibrium is not achieved and the susceptibilities do not conform rigorously to Boltzmann distribution over thermally populated low- and high-spin states. It is possible to fit the data quantitatively in the range 4.2–160 K by calculating χ_{Fe} simply in terms of summation of the high-spin fraction, β, and a low-spin fraction, according to the equation

$$\chi_{Fe} = \beta\chi_{HS} + (1 - \beta)\chi_{LS} \qquad (6)$$

The high-spin susceptibility, χ_{HS}, was calculated as before by using the matrix diagonalization based on the spin Hamiltonian of eq 3, while the low-spin susceptibility, χ_{LS}, was calculated from the observed ESR g values, viz. 2.78, 2.0, and 1.4. The latter method was based on the energy level scheme commonly employed in interpreting the ESR spectra of low-spin ferric porphyrins.[56] It utilizes four parameters, viz. λ, the spin–orbit coupling constant, Δ, the tetragonal splitting of the t_{2g} set, V, the rhombic splitting,[5,76,77] and κ, the orbital reduction factor.

Application of eq 6 to a true thermal equilibrium should lead to a variation in β with temperature obeying Boltzmann statistics and hence to linear log K vs. T^{-1} plots. This is the case in solutions of various azido iron(III) porphyrins and azido ferriheme systems.[56,78,79] It is not the case in the present polycrystalline sample, however, where we find that β is almost independent of temperature in the range 4.2–160 K. A good fit of χ_{obsd} to χ_{Fe} in this range is obtained (Figure 15) for a β value of 0.22. The other parameters are as follows: high-spin molecules (22.4%), $D = 5$ cm^{-1}, $E = 0.02 \pm 0.02$ cm^{-1} (i.e. $E/D \approx 0.004$); low-spin molecules (77.6%), $\lambda = -340$ cm^{-1}, $\Delta = 1320$ cm^{-1}, $V = 606$ cm^{-1}, $V/\Delta = 0.46$, $\kappa = 0.83$. While at first glance this may seem to be a case of overparameterization for minimal input data, it should be remembered that the low-spin parameters are fixed by the observed ESR g values, while the D and E values of the high-spin fraction give rise to the rapid decrease in μ_{Fe} at very low temperatures. These zero-field splitting parameters are compatible with the observed $g = 6$ line in the ESR spectrum. The low-spin parameters are similar to those of many other six-coordinate Fe(III) porphyrins.[55,56,58,76,77]

The magnetic analysis of the 4.2–160 K data means that the ratio of high- to low-spin molecules is effectively constant, since the kinetics of the spin crossover are very slow. Between 160 and 300 K the gradual rise in μ_{Fe} is consistent with an increase in the number of high-spin molecules.

As in the cases of the other $FeX(P\text{-}N_4)$ compounds, it is possible only to speculate on the chemical or structural reasons responsible for the spin crossover in this azido derivative. It may again relate to the presence, absence, or thermal motion of the molecule of methanol in the crystal lattice or the positional isomerism of the azido ligand. On the other hand, it could be a feature of the azido ligand, since as noted already, there are a number of Fe(III) porphyrin systems known to display crossover behavior.[56,78,79] It might have been informative to delineate the role of the solvent in this and other $FeX(P\text{-}N_4)$ complexes by a full magnetochemical investigation of the desolvated species. This remains for the future.

Solution Behavior. In contrast to the complex properties exhibited in the solid state, the solution properties are more consistent with those associated with simpler and more thoroughly studied high- and low-spin Fe(III) porphyrin derivatives.

In $CHCl_3$, 10% MeOH–90% $CHCl_3$, and Me_2SO frozen solutions at 4.2 K, the X-band ESR spectra of $FeX(P\text{-}N_4)$ for X = Cl, Br, OH all exhibit signals typical of tetragonal high-spin Fe(III) porphyrins such as Fe(TPP)Cl.[80] A typical example of $FeOH(P\text{-}N_4)$ in Me_2SO is shown in Figure 13. Although under certain conditions the presence of rhombic distortion is manifested by a small splitting of the $g_\perp$ signal, the spectra generally indicate axial symmetry expected for a pure single compound. Nevertheless, the ESR spectrum of $FeN_3(P\text{-}N_4)$ in 10% MeOH–90% $CHCl_3$ solution at 4.2 K exhibits features of both high and low spin states on Fe; in addition to the characteristic high-spin resonances at $g \approx 6$ and 2, there is also evidence of approximately 10% of a low-spin-state Fe(III) porphyrin with g values 2.78, 2.04, and 1.42.

(76) Rhynard, G.; Lang, G.; Spartalian, K.; Yonetani, T. *J. Chem. Phys.* **1979**, *71*, 3715.
(77) Smith, T. D.; Pilbrow, J. R. In "Biological Magnetic Resonance"; Berliner, L. J., Reuben, J., Eds.; Plenum Press: New York, 1980; Chapter 3.
(78) See, for instance: Ochiai, E. I. "Bioinorganic Chemistry, An Introduction"; Allyn and Bacon: Boston, 1977; Chapter 5 and references therein.
(79) See, e.g.: Neya, S.; Morishima, I. *J. Am. Chem. Soc.* **1982**, *104*, 5688 and references therein. Neya, S.; Morishima, I. *Biochemistry* **1980**, *19*, 258. Huang, Y. P.; Kassner, R. J. *J. Am. Chem. Soc.* **1979**, *101*, 5807.
(80) Subramanian, J. In "Porphyrins and Metalloporphyrins"; Smith, K. M., Ed.; Elsevier: New York, 1975; Chapter 13.

Table X. UV-Visible Maxima (nm) for Complexes $FeX(P\text{-}N_4)$ and $[Fe(P\text{-}(NO)_4)]_2O$ in Various Solvents

	CH_2Cl_2	10% MeOH–90% $CHCl_3$	Me_2SO
$FeCl(P\text{-}N_4)$	422, 512, 580, 653, 675	422, 508, 575, 645, 670	400 (sh), 422, 498, 530, 574, 625, 677
$FeBr(P\text{-}N_4)$	398 (sh), 422, 515, 586, 660, 687	398 (sh), 421, 514, 588, 660, 690	404 (sh), 422, 505, 531, 578, 650, 677
$FeN_3(P\text{-}N_4)$	*a*	420, 500 (sh), 582 (sh), 640 (sh)	400 (sh), 431, 500, 531, 578, 633, 675
$FeOH(P\text{-}N_4)$	422, 580, 620 (sh)	421, 585, 630 (sh)	422 (sh), 428, 578, 620;[b] 422, 498 (sh), 529, 572, 615, 675[c]
$[Fe(P\text{-}NO)_4)]_2O$	415, 572, 613	416, 573, 612	*a*

[a] Insoluble. [b] Fresh solution. [c] Aged solution.

This is in contrast to the solid-state spectrum, where the relative proportions of the high- and low-spin species are reversed.

At room temperature, solutions of these complexes also exhibit features that are indicative of the presence of a single high-spin species. The NMR spectrum of $FeCl(P\text{-}N_4)$ in 5% CD_3OD–95% $CDCl_3$ shows a single pyrrole resonance at 79.5 ppm downfield from Me_4Si, a position diagnostic of high-spin Fe(III) porphyrins.[81] Evan's method magnetic susceptibility measurements on $FeX(P\text{-}N_4)$, X = Cl, Br, OH, in $CHCl_3$ solution at 30 °C all give $\mu_{eff} = 6.0\ \mu_B$, which is the value expected for an $S = {}^5/_2$ system. The measured value for $FeN_3(P\text{-}N_4)$ in 10% MeOH–90% $CHCl_3$ is slightly lower at 5.8 μ_B, consistent with the presence of a small proportion of low-spin species as observed in the frozen-solution ESR spectrum.

The UV–visible maxima of the complexes in various solvents are given in Table X, and typical examples are illustrated in Figure 18. Similarities between the spectra of $FeX(P\text{-}N_4)$, X = Cl, Br, N_3, in potentially coordinating (Me_2SO) and noncoordinating (CH_2Cl_2) or weakly coordinating (MeOH–$CHCl_3$) solvents are obvious, and so too is the resemblance of the spectra of those of typical high-spin porphyrins such as Fe(TPP)Cl in the same solvents.[82] This suggests that both faces of the metalloporphyrin are accessible to coordinating ligands such as Me_2SO and the halide or azide is displaced by a solvent molecule to give the (presumably) six-coordinate high-spin complex. The $FeN_3(P\text{-}N_4)$ complex in 10% MeOH–90% $CHCl_3$ solution, however, exhibits a broad and rather featureless spectrum, again giving evidence of a mixture of high- and low-spin species in this solvent at ambient temperatures.

In the presence of strong-field ligands such as 1-methylimidazole, six-coordination to form the low-spin species also indicates minimal hindrance to approach from the face of the porphyrin containing the pyridine pickets. For example, in the potentially stepwise conversion of the high-spin complex $FeCl(P\text{-}N_4)$ in Me_2SO to the low-spin bis(1-methylimidazole) adduct

$$[Fe(Me_2SO)_2(P\text{-}N_4)]^+ + N\text{-MeIm} \rightleftharpoons [Fe(Me_2SO)(N\text{-MeIm})(P\text{-}N_4)]^+ + Me_2SO \quad K_1$$

$$[Fe(Me_2SO)(N\text{-MeIm})(P\text{-}N_4)]^+ + N\text{-MeIm} \rightleftharpoons [Fe(N\text{-MeIm})_2(P\text{-}N_4)]^+ + Me_2SO \quad K_2$$

isosbestic points are maintained at 608, 542, and 482 nm during a titration with *N*-MeIm, and analysis of the thermodynamic data by the procedure of Fleischer and Fine[83] indicates that only the overall reaction

$$[Fe(Me_2SO)_2(P\text{-}N_4)]^+ + 2N\text{-MeIm} \rightleftharpoons [Fe(N\text{-MeIm})_2(P\text{-}N_4)]^+ + 2Me_2SO$$

is observed, i.e., $K_2 >> K_1$, and the overall equilibrium constant

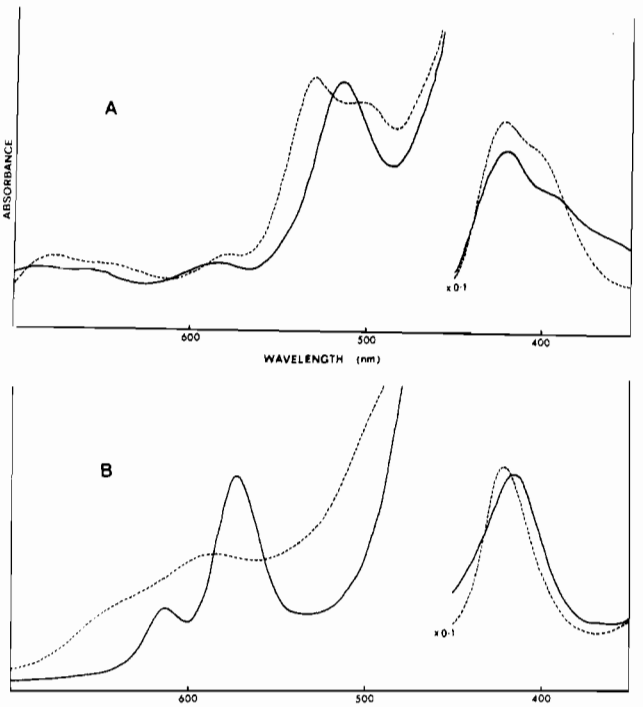

Figure 18. UV–visible spectra of (A) $FeBr(P\text{-}N_4)$ in CH_2Cl_2 (—) and Me_2SO (---), (B) $[Fe(P\text{-}(NO)_4)]_2O$ (—) and $FeOH(P\text{-}N_4)$ (---) in $CHCl_3$. From 700 to 450 nm the cell path length was 1.0 mm, and from 450 to 350 nm, 0.1 mm.

β_2 at 25 °C is 3.1×10^4, where $\beta_2 = [Fe(N\text{-MeIm})_2(P\text{-}N_4)]/[Fe(Me_2SO)_2(P\text{-}N_4)][N\text{-MeIm}]^2$ (cf. β_2 at 25 °C in Me_2SO for Fe(TPP)Cl, 1.28×10^4, and for hemin, 2.44×10^4).[81]

On the other hand, the UV–visible spectra of the hydroxo complex $FeOH(P\text{-}N_4)$ more closely resemble those of typical μ-oxo oligomers such as $(FeTPP)_2O$.[27] However, as illustrated in Figure 18, direct comparison with the spectrum of the tetra-*N*-oxide $[Fe(P\text{-}(NO)_4)]_2O$, prepared as indicated in the Experimental Section, reveals obvious differences. Ligand-binding studies also contrast the behavior of the hydroxo complex to that of the other high-spin complexes and the μ-oxo oligomer of the derived tetra-*N*-oxide.

Freshly prepared solutions of $FeOH(P\text{-}N_4)$ in CH_2Cl_2, MeOH–$CHCl_3$, and Me_2SO exhibit similar concentration-independent UV–visible spectra, suggesting the presence of a common five-coordinate or six-coordinate (polymeric) species in these solvents. However, in Me_2SO solution, a slow change in the spectrum is observed over several days, and the final spectrum closely resembles that of, e.g., $FeCl(P\text{-}N_4)$ in the same solvent. Presumably, the aging process involves slow displacement of the OH^- from the pocket to form the six-coordinate $[Fe(Me_2SO)_2(P\text{-}N_4)]^+$ species. Titration of a freshly prepared solution of $FeOH(P\text{-}N_4)$ in Me_2SO with *N*-MeIm does not proceed isosbestically, in contrast to the aged solution, which maintains isosbestic points at 604, 542, and 479 nm, and the final spectrum in each case is very similar to that obtained after titration of $FeCl(P\text{-}N_4)$ with *N*-MeIm,

(81) La Mar, G. N.; Walker, F. A. In "The Porphyrins"; Dolphin, D., Ed.; Academic Press: New York, 1979; Vol. IV, Chapter 2.
(82) Pasternack, R. F.; Gillies, B. S.; Stahlbush, J. R. *J. Am. Chem. Soc.* **1978**, *100*, 2613.
(83) Fleischer, E. B.; Fine, D. A. *Inorg. Chim. Acta* **1978**, *29*, 267.

Scheme II

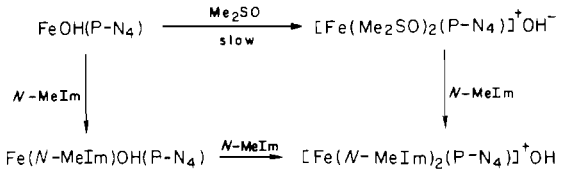

in accordance with Scheme II. The aging process in Me_2SO does not produce an overall spin-state change on Fe, as evidenced by the fact that the magnetic moment as measured by the Evans method is unchanged at 6.0 μ_B, and the ESR spectra of fresh and aged solutions at 4.2 K show identical $g \approx 6$, 2 spectra.

Although the μ-oxo oligomer $[Fe(P\text{-}(NO)_2)]_2O$ is insoluble in Me_2SO, solutions in $CHCl_3$ show little affinity for ligands such as *N*-MeIm, with an estimated $\beta_2 < 10^{-10}$ (cf. $\beta_2 = 65$ for the hydroxo complex in this solvent).

Conclusion

The series of compounds $FeX(P\text{-}N_4)$ has been shown to exhibit a diversity of magnetic behavior. Although a crystal structure of the Cl^- complex indicates an essentially high-spin character on Fe, albeit with an unusual axial ligand combination, it is clear that magnetically this series of complexes is finely balanced near the spin-crossover point. Subtle variations in axial ligand and solvation appear to be sufficient to affect the spin state on Fe, at least in the solid state. The solution behavior, on the other hand, is more clearly defined. With a detailed understanding of the magnetic properties of these complexes now established, an interpretation of the behavior of the heteronuclear complexes $Fe(P\text{-}N_4)XCu^{2+}$ is now possible and will be reported subsequently.

Acknowledgment. K.S.M. wishes to acknowledge grants from the Australian Research Grants Scheme and the Monash University Special Research Fund. Support from Professor David A. Buckingham and Professor Lewis N. Mander in the initial stages of this work is appreciated.

Registry No. $(FeCl(P\text{-}N_4))_n \cdot CHCl_3 \cdot H_2O$, 88082-42-2; $FeCl(P\text{-}N_4)$, 88082-44-4; $(FeBr(P\text{-}N_4))_n$, 88035-69-2; $FeBr(P\text{-}N_4)$, 88082-45-5; $(FeOH(P\text{-}N_4))_n$, 88082-43-3; $FeOH(P\text{-}N_4)$, 88082-46-6; $FeN_3(P\text{-}N_4)$, 88035-70-5; $[Fe(P\text{-}(NO)_4)]_2O$, 88035-71-6; $(P\text{-}N_4)$, 66887-83-0; *meso*-$\alpha,\alpha,\alpha,\alpha$-tetrakis(*o*-aminophenyl)porphyrin, 68070-27-9; nicotinic anhydride, 16837-38-0; trimethylamine *N*-oxide, 1184-78-7.

Supplementary Material Available: Tables of observed and calculated structure factors and of least-squares planes and Tables V, VII-IX showing observed susceptibility data (23 pages). Ordering information is given on any current masthead page.

Contribution from the Istituto FRAE—CNR, Bologna, Italy, Istituto di Scienze Chimiche della Facoltà di Farmacia and Istituto Chimico "G. Ciamician", Università di Bologna, Bologna, Italy, and Centro CNR sulla Fotochimica, Università di Ferrara, Ferrara, Italy

Photophysical Characterization of the Decatungstoeuropate(9-) Anion

ROBERTO BALLARDINI,[1a,b] QUINTO GIULIANO MULAZZANI,[1b] MARGHERITA VENTURI,[1c] FABRIZIO BOLLETTA,[1d] and VINCENZO BALZANI*[1b,d]

Received April 1, 1983

As a part of an investigation on completely inorganic photosensitizers, the photophysical properties of $EuW_{10}O_{36}^{9-}$ have been fully characterized. The absorption spectra, emission spectra (under low and high resolution), and emission decay of $EuW_{10}O_{36}^{9-}$ under a variety of experimental conditions (solid state, H_2O or D_2O solutions of different concentrations with or without the addition of neutral salts, rigid matrix at 77 K) are reported. On the basis of the results obtained concerning the number of $^5D_0 \rightarrow {}^7F_0$ bands under high resolution, the splitting of the $^5D_0 \rightarrow {}^7F_J$ bands, and the decay of the emission intensity, the following is shown: (i) in aqueous solutions $EuW_{10}O_{36}^{9-}$ maintains its integrity, but it is subjected to equilibria involving the coordination of water molecules to europium, the acid dissociation of coordinated water, and the formation of ion pairs with the cations present in solution; (ii) in very diluted solutions the predominant excited-state species contains four coordinated water molecules and possesses C_{4v} symmetry; the lifetime of the $^5D_0$ emitting state is 0.25 ms in H_2O and 3.7 ms in D_2O, showing that the main radiationless deactivation process involves coupling with OH oscillators; (iii) increasing ionic strength causes the appearance of more strongly emitting and longer lived species that contain fewer coordinated H_2O molecules; (iv) in the solid state only one $EuW_{10}O_{36}^{9-}$ species is present, which exhibits D_{4d} symmetry and whose lifetime is 3 ms regardless of whether it has been crystallized from H_2O or D_2O, showing that no water molecule is coordinated to Eu^{3+}; (v) emission can be obtained upon excitation of both the weak $f \rightarrow f$ bands in the visible and the strong bands in the UV region, which are attributed to $O \rightarrow W$ charge-transfer transitions within the $W_5O_{18}^{6-}$ "ligands"; (vi) the emission quantum yield in D_2O solution is 0.5 on excitation at 394 nm ($^5L_6$ level) and 0.2 on excitation at 250 nm ($O \rightarrow W$ charge transfer). The possible use of $EuW_{10}O_{36}^{9-}$ as a photosensitizer is briefly discussed.

Introduction

Photochemical conversion of solar energy by redox cycles in homogeneous solution is based on photosensitizer and relay species that must induce and mediate electron-transfer steps of a thermodynamically uphill reaction.[2] For example, the splitting of water by solar energy has been reported to occur when $Ru(bpy)_3^{2+}$ (bpy = 2,2'-bipyridine) and methylviologen are used as a photosensitizer and relay species, respectively.[3] Most of the molecules proposed so far as photosensitizers and relays for such energy-conversion processes are organic compounds or transition-metal complexes containing aromatic ligands. These molecules usually do not show long-term stability in the reaction medium because they may be involved

* To whom correspondence should be addressed at the Istituto FRAE—CNR.

(1) (a) Centro CNR sulla Fotochimica. (b) Istituto FRAE—CNR. (c) Istituto di Scienze Chimiche. (d) Istituto Chimico "G. Ciamician".
(2) (a) Connolly, J. S., Ed. "Photochemical Conversion and Storage of Solar Energy"; Academic Press: London, 1981. (b) Rabani, J., Ed. "Photochemical Conversion and Storage of Solar Energy"; Weizmann Science Press: Jerusalem, 1982. (c) Balazani, V.; Scandola, F. In "Energy Resources by Photochemistry and Catalysis"; Graetzel, M., Ed.; Academic Press: London, 1983; p 1.
(3) Graetzel, M. *Acc. Chem. Res.* **1980**, *14*, 376.

0020-1669/84/1323-0300$01.50/0